Experimental study on strengthening of RC beams with Side Near Surface Mounted technique-CFRP bars

Mohammad Abdallah, Firas Al Mahmoud, Rémi Boissiere, Abdelouahab Khelil, Julien Mercier

Experimental study on strengthening of RC beams with Side Near Surface Mounted technique-CFRP bars

Mohammad Abdallah*(1), Firas Al Mahmoud(1), Rémi Boissière(1), Abdelouahab Khelil(1) and Julien Mercier(2)

(1)Institut Jean Lamour, UMR 7198, CNRS, Université de Lorraine, Nancy, France
(2)Freyssinet, Paris, France

**Corresponding Author: Mohammad Abdallah. Université de Lorraine, mohammad.abdallah@univ-lorraine.fr*

Abstract: This paper presents an experimental program that was carried out for the purpose of studying the global flexural performance of reinforced concrete beams strengthened internally with Carbon Fiber Reinforced Polymer (CFRP) rods using the Side Near Surface Mounted (SNSM) technique. The CFRP rods were placed laterally, adjacent to the longitudinal steel bars inside precut grooves. The strengthening length and position of CFRP rods as well as the type of filling material were the main variables investigated in this study. Moreover, a detailed comparison between the Side Near Surface Mounted (SNSM) and the Near Surface Mounted (NSM) techniques for the strengthening of RC beams using CFRP rods was conducted as well; in order to validate and assess the effectiveness of the SNSM technique.
The test results showed that using the SNSM-CFRP rods technique allowed improving in a significant way the load carrying capacity of RC beams but decreased their ductility along the deflection at maximum load. The results obtained indicated that the failure mode was influenced by the length of CFRP rods and the filling material characteristics, while the strengthening position did not have significant impact. The SNSM strengthening technique can be used as an alternative method to the NSM method, and in some cases, it may be used to prevent the non-conventional failure modes, due to degradation of the NSM strengthening system, such as the pull out of CFRP-rods or premature debonding failure. The conventional analytical model accurately predicted the strength capacity and mid-span deflection of the SNSM strengthened beams.

***Key words**: CFRP rods, SNSM reinforcement, experimental, RC beam, flexural behavior.*

1 Introduction.

Since the 1990s, the degraded reinforced concrete (RC) structures due to exposure to natural hazards and extreme weather events have been repaired with the help of Fiber Reinforced Polymers (FRPs). A wide range of studies have been conducted on strengthening or retrofitting RC elements using externally bonded (EB) FRP laminates or/and sheets [**1-4**]. Despite the mechanical strengthening advantages of using the EB-FRP technique, some drawbacks, which

represent genuine handicaps in its practical execution and long-term monitoring, still exist. For instance, one can mention the pretreatment process, installation time, premature debonding failure due to interfacial stresses, and the mechanical damages resulting from accidental impacts.

In the past ten years, the Near Surface Mounted (NSM) technology is viewed as a promising alternative to the externally bonded (EB) FRP strengthening technique; this is actually a prevailing method for strengthening existing concrete structures using FRP reinforcement [5]. The NSM technique has attracted worldwide attention due to the different advantages it offers: (1) The NSM-FRP system is quite simple and does not require extensive surface preparation work. The FRP composites (rods, strips, etc) are inserted adjacent to longitudinal steel bars and embedded inside precut grooves in the beam soffit; they are bonded to concrete with epoxy-based pastes or modified cement grouts [6]; (2) RC members strengthened with NSM-FRP reinforcement proved to be much more ductile and experienced failure at much higher level as compared to EB-FRP members [7,8]; (3) Strengthening of RC components with the NSM technique offers higher bonding efficiency and better protection for the FRP reinforcement as compared to the EB strengthening technique [9].

Several experimental studies investigating the NSM-FRP technique have underlined its potential for strengthening reinforced concrete (RC) beams. **Almahmoud et al. [6,10]** found that the NSM method, using CFRP rods, can significantly improve the ultimate strength of RC beams by 50%, at least, over the ultimate strength of non-strengthened beam. Their experimental results also indicated that the failure mode of strengthened beam varies from degradation of the CFRP rod mounting to compressive concrete crushing and depends on the ratio of a combination of CFRP cross-section and length to the concrete compressive strength. **Kreit et al. [11]** presented a testing program for the purpose of assessing the flexural performance of corroded RC beams strengthened with CFRP rods using the NSM method. The experimental results showed that retrofitted beams with 36% loss in steel cross section displayed an ultimate capacity similar to that of an un-corroded control beam. Moreover, two types of failure modes were observed; one was due to failure of the tension corroded steel and the other was because of concrete cover peeling off at level of the additional reinforcement (CFRP). **Sharaky et al. [12]** investigated the flexural performance of NSM strengthened RC beams with partially and fully bonded CFRP and GFRP bars. The specimens strengthened with fully bonded reinforcement showed higher stiffness and greater bearing capacity than those strengthened with partially bonded reinforcement. Also, the concrete cover separation was the dominant failure mode regarding the NSM-CFRP rods beams. On the other hand, the fully bonding NSM-GFRP rods beams failed due to either deboning at the concrete-epoxy interface or concrete splitting, depending on the number of grooves used. Furthermore, **Khalifa [13]** made an attempt to assess the effectiveness of NSM and EB systems with CFRP reinforcement for the purpose of improving the flexural strength of RC beams under four-point loading. The beams strengthened with NSM-CFRP strips exhibited higher ultimate loads than those strengthened with EB-CFRP sheets; the difference ranged from 12% to 18%. The tested NSM beam specimens failed due to debonding of the CFRP strips along with concrete cover peeling off. For their part, **Sebastian et al. [14]** evaluated the

structural performance of indeterminate RC beams internally reinforced with NSM-CFRP rods. The strengthened structure failed due to the peeling-off of CFRP bars in the positive moment region; in addition, the ultimate load carrying capacity of the strengthened beam was 37% higher than that of the control beam.

Although the above mentioned studies have indicated that NSM-FRP reinforcement can significantly enhance the flexural behavior of RC beams by increasing their ultimate capacity; this strengthening system might not be feasible in several practical cases, especially when the building is operating. In this case, widths of the beams are usually occupied by partitions as masonry walls. In other cases, the NSM technique presents some restrictions in its application : (1) Only a limited number of FRP bars can be used in each specimen, on account of the effective groove spacing. The minimum clear spacing (SG) between grooves (**Fig.1**) should be greater than twice the depth of the groove, otherwise debonding failure may occur due to stress overlapping [**6**,**15**,**16**]; (2) Application of the NSM technique might be difficult or even impossible for some parts of structures, particularly, over the supports. Applying anchorage of FRP rods over the supports in RC beams cannot be easily performed and could impact other structural components, such as columns and joints, during preparation and/or installation; (3) The bond efficiency of NSM-FRP rods is substantially associated with the quality of the concrete cover; for instance, in corroded beams, the bottom concrete cover is highly exposed to damage due to corrosion of the longitudinal steel bars, particularly when steel bars are arranged in one layer, and therefore, putting FRP rods in such places may reduce their expected additional resistance and drive to premature failure [**11, 17**]; hence, a need to change the strengthening position becomes essential. (4) As stated in the above-mentioned literature, application of NSM-CFRP technique for strengthening RC beams could lead to non-conventional failure modes, i.e. peeling off and pull out failures modes, due to degradation of the strengthening system, which induces a significant reduction in the ductility of beams [**9-14**,**18-20**]. Thus, in order to overcome the NSM limitations or/and its operational obstacles, the Side Near Surface Mounted (SNSM) technique has recently been proposed as a new alternative approach for strengthening reinforced concrete (RC) members using fiber reinforced polymer (FRP) reinforcing bars. In this proposed technique the FRP elements inserted in the vertical sides of the beam instead of the bottom side. The use of the SNSM method is quite recent and very few researchers have investigated the subject so far. Indeed, **Akter et al [21]** examined the structural behavior of RC beams strengthened with CFRP and steel reinforcing bars using the SNSM technique. Although the main variable studied was the additional reinforcement ratio, the test results indicated that applying 2Ø8, 2Ø10 and 2Ø12 SNSM-CFRP rods could increase the flexural strength of beams by up to 91%, 138% and 133% ,respectively, over the non-strengthened control beam. The impact of other variables, such as the CFRP length, CFRP position and type of filling material have still not been extensively studied yet. Therefore, the purpose of the present work is to investigate the global behavior of reinforced concrete beams strengthened with 2Ø6 CFRP rods using the SNSM technique. This was carried out by studying three key parameters that are likely to affect the structural response, namely, strengthening length, strengthening position and filling

material characteristics. A detailed comparison between the SNSM and NSM strengthening approaches was performed in terms of the failure and bearing capacity mechanisms. In addition, the test results obtained were compared with those of conventional analytical models; also, the computed flexural strength capacity and mid-span deflection of the strengthened beams were found to be in good agreement with the experimental ones.

2 Experimental program

2.1 Test beams and materials.

A total of six RC rectangular beams, including one control beam (CB), were tested to failure by applying monotonically increasing four-point bending loads. The RC beams were designed to experience flexural failure in accordance with the ACI code [**15**]; they were reinforced with two ordinary 12-mm-diameter deformed steel bars in the tension zone and two 6-mm-diameter ribbed bars in the compression zone. The deformed steel bars in the compression zone were utilized as hanger bars; and they were running along the shear zones. Closed 6-mm-diameter stirrups were provided against the maximum shear with a 150-mm center-to-center spacing. The concrete cover thickness in all tested beams was maintained at 20-mm for the vertical sides and 30-mm at the top and bottom sides. The beam geometry and steel reinforcement configuration are illustrated in **Fig. 2**.

The characteristics of concrete employed in the formulation of RC beams were determined by laboratory testing of three hardened concrete cylinder specimens (D = 160 mm and H = 320 mm). The average compressive and tensile strengths as well as the modulus of elasticity of concrete at 28 days were 37.0MPa, 3.0MPa and 30.3Gpa, respectively. However, in order to determine the mechanical properties of longitudinal steel bars, two steel bar specimens of diameter 12-mm were tested in tensile and the measured yield strength was 600MPa, and the modulus of elasticity was 210GPa.

Five beams were internally strengthened in bending with two 6-mm-diameter CFRP rods (56.5mm2) installed into two grooves, i.e. one rod in each groove, using the SNSM technique (**see Fig. 2**). The longitudinal grooves ($12 \times 12\text{mm}$) were made with a special concrete saw. In addition, in order to ensure proper bonding between the filling material and concrete substrate, it was decided to apply an airbrush at high pressure to remove debris and fine particles. The grooves were filled up to two stages so to guarantee that the filling material is in-full contact with the surface of CFRP bars. Afterwards, all strengthened beams were confined at room temperature (T = 20 °C) for one week in order to obtain maximum strengthening level, depending on the filling material used, before testing.

The mechanical properties of the strengthening material were determined through axial testing of three CFRP rods by [**22**]. The CFRP rods tested exhibited dissimilar response to that of the conventional steel bars, principally, the linear-elastic attitude up to the failure point (brittle

failure). The ultimate tensile strength and Young's modulus of the CFRP rods used were 1875MPa and 146GPa respectively.

Two types of groove-filling materials for bonding the CFRP bars to the internal concrete surface were considered in this research, namely epoxy resin and mortar. **Table 1** shows the compressive and tensile strengths of the epoxy resin and mortar at 7 days. The compressive and tensile strengths of resin were according to the manufacture, whereas the mechanical properties of mortar were determined by laboratory testing of four specimens.

2.2 Beam strengthening

Each strengthened beam was assigned a reference code that defines its strengthening scenario. For example, BC1(270-SR) means that beam BC1 is strengthened with 270-cm-long CFRP bars placed alongside the steel bars (S) and embedded in resin filling material (R).

However, the strengthening scheme of this study was designed to investigate the effectiveness of the SNSM-CFRP technique in upgrading the flexural capacity of RC beams. Therefore, the global flexural performance of the series beams BC1(270-SR), BC2(210-SR), BC3(270-SM) and BC4(210-SM), was studied with respect to the running length of CFRP rods and the type of filling material. The CFRP rods used to strengthen the above four beams were placed at the same level as the tensile steel (about 42-mm from the beam bottom surface). Beams BC1(270-SR) and BC3(270-SM) were strengthened with 270-cm-long CFRP bars, whereas 210-cm-long CFRP bars were employed in strengthening beams BC4(210-SM) and BC2(210-SR). The CFRP bars were embedded in resin in the case of beams BC1(270-SR) and BC2(210-SR); however, for beams BC3(270-SM) and BC4(210-SM), these bars were inserted into mortar.

Furthermore, another RC beam, namely BC5(270-UR), was strengthened with two 6-mm-diameter CFRP rods embedded in resin and placed 20-mm higher than the longitudinal steel bars level (about 62-mm from the beam bottom surface), **Fig. 2**. The purpose was to assess effects of the position of CFRP rods on the flexural response of the beam. Indeed, the efficiency of the SNSM technique is substantially influenced by the quality of the concrete cover. Thus, a need to change the strengthening position in some competitive conditions might prove essential to ensure sufficient concrete cover for groove preparation and CFRP rebar installation. The flexural response of beam BC5(270-UR) was compared with that of beam BC1(270-SR). The test matrix of this study are summarized in **Table 2**.

2.3 Instruments and test procedure.

All beams were tested under four-point loads up to failure. The main load (P) was applied using a hydraulic actuator with capacity of 400 kN and 0.3 kN/s average loading speed. The total applied load was measured by means of an attached electrical load cell. A steel beam was utilized to distribute the total applied load into two concentrated loads. Each load (P/2) acted at a point situated at 80 cm from the adjoining support.

A vertical linear variable differential transducer (LVDT) was used for each tested beam in order to monitor the vertical mid-span deflection. Regarding the strengthened beams, four

electrical strain gauges in total were used for each specimen for the purpose of monitoring the strain in the internal tensile steel bars and the adjacent CFRP rods. The strain gauges were attached to midpoint of reinforcement bars and oriented in the longitudinal direction. They were well protected with three different layers (protective paste, rubber piece and aluminum tape) after coated with polyurethane material to ensure high degree of measuring accuracy. **Fig. 3** illustrates the set up and instrumentation of beams.

3 Results and discussion

3.1 load-deflection response

Figure 4 illustrates the curves representing the total applied load versus the mid-span deflection for the tested beams. In general, the load carrying capacities of RC beams strengthened with CFRP bars using the SNSM technique were greater than the load carrying capacity of the control beam, CB. The overall load-deflection response $(P-\delta)$ indicates that the tested beam specimens went through three distinct stages: elastic or pre-cracking stage (O-A), concrete cracking stage (A-B) and ultimate strength stage (B-C).

It should be clearly noted that in the elastic phase, all the beams displayed the same linear behavior and this is because of the flexural rigidity of beams as well as the bonding between the filling material and concrete were not yet been affected. The potential of CFRP rods to enhance the cracking strength of beams was negligible. The first turning point (A) represents the end of this phase, particularly, when concrete starts cracking.

In the concrete cracking stage, the slopes of strengthened beams were higher than the slope of control beam (A-B lines), which may be attributed to the fact that the CFRP bars improved the stiffness and yield load of the beams. As expected, the horizontal fine cracks on the leveled surface of grooves as well as the flexural cracks in the constant moment zone were observed in this stage. Note that these cracks spread and widened as the external load increased. The cracking phase ended at the second turning point (B), which represents the steel yielding load.

In the ultimate strength phase, the considerable change in slope of the $(P-\delta)$ curves as compared to the slopes in the two previous phases, was due to the intrinsic drop in the elastic modulus of tension reinforcement. It is apparent, however in this stage, that all strengthened beams presented higher load-increasing rates than that of the control beam (CB), which implies that the additional reinforcement, provided by the CFRP rods, controlled the flexural performance of the RC beams after the yielding point of tension steel was reached. At the third turning point (C), which represents the end of the ultimate strength stage, the RC beams strengthened with SNSM-CFRP rods exhibited lower ultimate mid-span deflections than that of the control beam.

3.2 Failure mods and cracking pattern

In addition to the conventional ductile flexural failure mode of the reference beam, CB (tensile steel yielding followed by concrete crushing at the beam mid-span); three different failure modes were observed in the SNSM-CFRP beams (concrete crushing in beams BC1(270-SR) and BC5(270-UR), debonding failure in beams BC3(270-SM) and BC4(210-SM) and concrete cover peeling off in beam BC2(210-SR)), as indicated in **Table 3.**

3.2.1 Failure mode 1

The two beams BC1(270-SR) and BC5(270-UR) experienced the same failure mode although they carried different peak loads. Failure was due to crushing of the brittle compressed concrete in the constant moment zone, close to one of the two load application points, after yielding of the tension steel reinforcement, as shown in **Fig. 5**.

In the initial loading stage, horizontal fine cracks were apparent in the resin region. Afterwards, as the applied load was increased, these cracks gradually merged to the flexural cracks which propagated from the bottom side of the tested beams to the load application point. The flexural cracks growth in this set of beams (BC1(270-SR) and BC5(270-UR)) was influenced by the CFRP rod location. The flexural cracks in beam BC5(270-UR) were wider than those in beam BC1(270-SR), which is basically attributed to the displacement of the CFRP rods position to 20-mm above the steel bar level. The new position of the CFRP reinforcing bars in BC5(270-UR) created a new tensile stress level, which consequently caused the cracks to widen further and therefore to expanded upwards. Indeed, the crack pattern of this set confirms that the SNSM-CFRP reinforcing bars worked effectively as an additional tensile reinforcement **[23]**.

However, conspicuous horizontal cracks appeared in the failure sections of both beams, as a result of compressed concrete splitting. These cracks progressively extended and widened in the direction of the mid-span.

3.2.2 Failure mode 2

The failure mode of beams BC3(270-SM) and BC4(210-SM) was characterized by debonding between the internal surface of the groove (concrete) and mortar, as shown in **Fig. 6**.

The debonding failure mechanism of this set of beams was particularly influenced by the length of CFRP rods. Instantaneous debonding failure suddenly occurred in beam BC4(210-SM), immediately after yielding of the tension steel. This was very abrupt and was followed by beam failure once the concrete at the top of the beam began to crush. On the other hand, the beam BC3(270-SM) continued to deflect but did not fail even after it reached its yielding load; it continued to resist external loads until concrete started crushing in the top fibers. At this point, cracking noises could clearly and continuously be heard, due to the mortar debonding from the concrete, until the failure load was reached. Note that the failure section of beam BC3(270-SM)

was observed at the mid-span, nearly the same way as for the control beam (CB); however, failure was observed close to the load application point for beam BC4(210-SM).

Regarding the cracking mechanism, the flexural cracks in beam BC4(210-SM) were narrow but more uniformly distributed than those in beam BC3(270-SM). On the other hand, the horizontal crack due to splitting of the compressed concrete was more conspicuous in beam BC3(270-SM). It is worth mentioning that the mortar-concrete interface was affected by internal longitudinal cracks, particularly at the failure sections. These cracks prevented the flexural cracks to cross the mortar in beam BC4(210-SM) or changed the flexural cracks direction in beam BC3(270-SM). This could be attributed to the debonding failure mechanism, as stated above in each beam **[24].**

3.2.3 Failure mode 3

The failure mode of beam BC2(210-SR) was certainly due to brittle concrete peeling-off in the region where maximum shear occurs; this was immediately followed by the beam failure, as shown in **Fig. 7**.

In the initial stage of loading, the crack pattern of beam BC2(210-SR) was almost similar to that observed in beams BC1(270-SR) and BC5(270-UR). As the applied load increased, shear cracks at the end of the additional reinforcement (CFRP bars) started to intersect the fine cracks which had previously appeared in the resin region. The intersection of the shear cracks with the minor horizontal cracks caused a significant main horizontal crack to develop and expend along the beam length at the same level as the CFRP rods. The intersection of the main horizontal crack with the bending vertical crack, which developed in the region close to the concentrated applied load, enhanced the peeling-off of the concrete cover over a significant length in the beam soffit, that is from the extremity of the CFRP bars to the region of maximum moment**.** In addition, one may clearly notice that visible flexural-shear cracks were formed over the failure length, particularly in the lower moment regions.

3.3 Enhancement of load carrying capacity of SNSM strengthened beams.

Table 3 summarizes the load carrying capacities of the tested beams representing the cracking load (P_{cr}), yielding load (P_y) and ultimate load (P_u). **Fig. 8** shows the load-strain curve of the SNSM-CFRP rods. It should be noted that the CFRP load-strain curve is nearly similar to the load-deflection curve (see **Fig. 4**). From **Fig. 8**, it can be seen that the CFRP rods have not taken much load up to the first crack as the strains were almost zero; their potential to enhance the cracking load of the strengthened beams compared to the control beam was negligible. Afterwards, the CFRP strain curves have shown reasonable inclinations, which means that the additional bars have started to carry substantial loads, and thus significantly improved the yielding and ultimate loads of the SNSM-CFRP beams. The CFRP strains exhibited nearly linear curves up to tension steel yielding load, thereafter the strains were gradually increased up to the failure load.

In the subsequent sections, however, the effectiveness of the SNSM technique in improving the yielding and ultimate load carrying capacities of RC beams strengthened with CFRP rods is discussed with respect to the strengthening length, strengthening position and filling material type. The ultiame load of tested beams was determined from the load–deflection curves (**Fig.4**), while the yielding load was detemined according to the strain gauge measurment (**Fig.9**, $\varepsilon_{y(exp)} \approx 0.29\%$, where $\varepsilon_{y(exp)}$ is the experimental yielding strain obtained from tensile test of the steel bars). It should be noted that the strain gauges installed on the steel rebar of beam BC3(270-SM) are stopped working during the loading process due to technical problem which may make the reported yielding load of this beam is not accurate.(see **Fig.9**)

3.3.1. Effect of the CFRP strengthening length

The tension steel in beams BC1(270-SR) and BC2(210-SR) yielded at about 90kN and 94.5kN, respectively, which represents an increase of 40% and 47% over the yielding load of the control beam. Beam BC1(270-SR) failed due to crushing of brittle compressed concrete at loading of 116 kN with an increase of about 59.3% in the failure load compared to the control beam, whereas beam BC2(210-SR) failed as a result of concrete peeling-off at loading of 106.4kN with an increase of 46.2% in the failure load. The maximum tensile strain measured on CFRP rods was 0.0069mm/mm for beam BC1(270-SR) and 0.0042mm/mm for beam BC2(210-SR); these values represent respectively about 53.9% and 32.8% of the ultimate strain of CFRP bars (see **Table 3**).

Regarding beams BC3(270-SM) and BC4(210-SM), the yielding started, respectively, at 81.8 kN, which is 27.2% greater than that of CB, and at 92.4 kN, which is 43.7% higher than that of CB. The load at failure was 106 kN for beam BC3(270-SM), and at 94.1kN for beam BC4(210-SM). These failure loads represent an increase of 45.6% and 29.3% with respect to CB. As stated in the failure mode section, the debonding failure, between the filling material and concrete, occurred at an earlier stage in beam BC4(210-SM) than in beam BC3(270-SM). The recorded strain of CFRP bars at failure was 0.0064 mm/mm for beam BC3(270-SM) and 0.0028 mm/mm for beam BC4(210-SM); these values represent, respectively, about 50% and 21.9% of the CFRP rod ultimate strain.

Consequently, increasing length of the CFRP bars led to increase the failure load of the beam and the maximum measured strain of the SNSM-CFRP bars. It was noted that 60-cm of supplementary length of the CFRP rods helped to avoid non-conventional failure mode (peeling-off) or delayed the debonding failure, and therefore, the CFRP rods worked more efficiently as an additional tensile reinforcement. In other words, it may be stated that increasing the ratio between the strengthening length *SL* (distance between the end of the CFRP bar and the applied load) and the beam length *BL* (distance between the support and the applied load) significantly enhances the flexural response of the SNSM-CFRP beam. The $\frac{SL}{BL}$ ratio of beams BC1(270-SR) and BC3(270-SM) was 0.94, whereas the $\frac{SL}{BL}$ ratio of beams BC2(210-SR) and BC4(210-SM) was 0.56. The failure load of BC1(270-SR) was about 9.1% grater than that of BC2(210-SR), and the

failure load of BC3(270-SM) was about 12.6% grater than that of BC4(210-SM). The variation between the yielding load of beams BC1(270-SR) and BC2(210-SR), which represents about 5% relative to BC1, may either refer to experimental results scattering or influence of the SNSM strengthening length, thus further experimental studies to investigate effects of the strengthening length of SNSM-CFRP bars on performance of RC beams are necessary.

3.3.1 Effect of the filling material

.

The failure mode of mortar beams; i.e. BC3(270-SM) and BC4(210-SM), was characterized by debonding between the filling material and concrete substrate, whereas no signs of debonding failure were observed in the resin beams; i.e. BC1(270-SR) and BC1(270-SR), (**section 3.2**). These findings are in good agreement with those reported in previous studies, on NSM-CFRP beams, which indicated that using resin as a filling material forms better bonding with concrete than using mortar [**6**]. Thus, the failure loads as well as the maximum measured strain of CFRP rods in mortar beams (**Table 3**) were lower than those in resin beams (BC3(270-SM) vs. BC1(270-SR) and (BC4(210-SM) vs. BC2(210-SR)).

3.3.2 Effect of the strengthening position

As can be seen from **Table 3**, beam BC5(270-UR) yielded at 83.2kN before the yielding load of beam BC1(270-SR) (difference about 6.8 kN). The beam BC5(270-UR) failed due to concrete crushing, which is similar to the failure mode of BC1(270-SR), at 102.7kN. Although, this value is about 41.1% higher than that of the control beam; it is also about 11.5% lower than the failure load of beam BC1(270-SR). The maximum tensile strain measured on CFRP rods was 0.0041mm/mm and this value represents about 32% of the CFRP ultimate strain (40.6% lower than the maximum recorded strain of CFRP rods in BC1(270-SR)).

Consequently, the slight drop in the yield and ultimate load carrying capacities of beam BC5(270-UR) compared with beam BC1(270-SR) was due to the fact that the CFRP rods in beam BC5(270-UR) caused an additional tensile stress above the steel bars level; and this led to decrease the effective moment arm of the tensile reinforcement (CFRP and steel bars) within the beam cross section.

3.4 Ductility

Design standards require adequate ductility in order to prevent brittle failure of RC members, and therefore provide warning of impending collapse. In this study, the displacement ductility index (μ) is obtained from the load-deflection response of the beam specimens (**Fig. 4**), and it is calculated according to the deflection computation as follows [**25**]:

$$\boldsymbol{\mu = \frac{\delta_u}{\delta_y}} \qquad \textbf{(1)}$$

The mid-span deflection, corresponding to the beam ultimate load $\boldsymbol{\delta_u}$ and yielding load $\boldsymbol{\delta_y}$, and the ductility index (μ) for the strengthened beams and control beam are given in **Table 4**.

In general, all the strengthened beams displayed less displacement ductility index (μ) compared to the non-strengthened beam; this is attributed to the increased tensile reinforcement (tension steel and CFRP bars). In fact, the ductility findings demonstrate effects of the brittle performance of CFRP rods and the SNSM strengthening approach as follows;

- Placing CFRP rods above the level of steel bars or using mortar instead of resin as a filling material proved to reduce the beam ductility. The decrease percent in μ-index of beams BC3(270-SM) and BC5(270-UR), with respect to the control beam, were about 45.1% and 33% respectively, whereas the decrease percent of BC1(270-SR) beam was 26.6%.
- The large reduction in ductility values of beams BC2(210-SR) and BC4(210-SM) was due to the insufficient strengthening length (210-cm), which led to non-conventional failure modes (peeling off or early debonding failure) as a result of degradation of the strengthening system. The percentages of decrease in the $\boldsymbol{\mu}$ index of beams BC2(210-SR) and BC4(210-SM) were found equal to 66.6% and 76.7%, respectively, with respect to the control beam (CB).

However, according to tension control design principle for reinforced concrete members, adequate ductility is achieved if the strain of steel (ε_s) at the point of concrete crushing or failure of the fiber reinforced polymer (FRP) is at least equal to 0.005 [**26**]. **Fig. 9** depicts the load-strain curves of the longitudinal tension steel in the tested beams. It can be noted that, using SNSM-CFRP rods significantly reduces tensile strains of the adjacent steel bars as compared to those in the control beam for the same applied load. The rate of increment was almost identical for all SNSM beams up to the yielding load. Afterwards, strains of the steel bars were rapidly increased but also influenced by the failure mode of the beam. It can also be found that, after the yielding load, inclinations of the load-strain curves of steel bars were lower than those of SNSM-CFRP bars for the same beam (see **Fig.8**); which implies that the SNSM bars controlled the flexural behavior up to the failure load. As can be seen from **Fig. 9;** beams BC1(270-SR) and BC5(270-UR) meet the ductility requirement ($\varepsilon_s > 0.005$). The measured tensile strains of the steel bars (**Table 3**) for beams BC1(270-SR) and BC5(270-UR) at the failure load were 0.0082-mm/mm and 0.0104-mm/mm, respectively.

Based on the steel tensile strain results; the displacement ductility index $\mu = 3$ represents the acceptable lower limit to guarantee ductile performance of the SNSM-CFRP bars strengthened beam. It should be noted that, this result corresponds to the range of μ-index, which was proposed by [**27**], in order to ensure the ductile behavior of RC beams ($3 \leq \mu \leq 5$). The ductile index of beams BC1(270-SR) and BC5(270-UR), obtained from Eq.(1), are within this reasonable range.

3.5 Energy absorption

The energy absorption capacity (E_{ab}) of RC beam could be defined as the area enclosed by the load-deflection curve (Table3). It indicates to the energy absorbed per unit cross-sectional area of the specimens calculated at any deflection extreme point [28]. **Fig.10** demonstrates influences of position and length of CFRP bars as well as the filling material type (resin or mortar) on the energy absorption capacity of the tested beams.

One observation was that, the strengthening length significantly influences the energy absorption capacity of strengthened beams compared to the other variables considered in this study. Compared to the control beam, 270-cm-long CFRP bars improved the energy absorption of the SNSM beam whatever the filling material used or position of the CFRP bars; the E_{ab} for beams BC1(270-SR), BC3(270-SM) and BC5(270-UR) increased by 69.6%, 9.2% and 20.9%, respectively. On the other hand, the energy absorption capacity of beams BC2(210-SR) and BC4(210-SM) decreased by 41.3% and 64%, respectively compared to the control beam. This considerable reduction in the E_{ab} of SNSM beams strengthened with 210-cm-long CFRP bars is principally due to their premature failure mode.

4 SNSM and NSM techniques: comparison and discussion.

Almahmoud et al. [6] carried out laboratory tests for the purpose of investigating the global behavior of reinforced concrete beams strengthened with CFRP rods using the Near Surface Mounted (NSM) technique. Their experimental work was performed on simply supported RC beams subjected to flexural loading and strengthened with CFRP rods. The study focused on changes, such as failure modes and enhancement of ultimate strengths, in the structural performance of RC beams. However, in the present work, the mechanical characteristics of the tested specimens and CFRP bars (length, section,..etc.) were cautiously selected, and the experimental setup was carefully designed in compliance with those used in the above mentioned study. This was done for the purpose of comparing the two strengthening techniques, NSM and SNSM. For this reason, the experimental results of the three NSM-CFRP beams, i.e. S-C 6 (270-R), S-C 6 (270-M) and S-C 6 (210-R), were utilized. More details about these beams can be found in [6].

Table 5 compares the experimental results obtained with the SNSM technique with those obtained with the NSM technique in terms of the failure mode, cracking, yielding and ultimate moments as well as the ductility index($\boldsymbol{\mu}$). **Figure 11** depicts the bending moment-deflection ($M-\delta$) curves of the tested SNSM beams as well as those of the NSM beams. The corresponding bending moment $M$of the beam is calculated by Eq.2.

$$\mathrm{M} = \frac{\mathrm{P}}{2} \times \mathrm{a} \qquad \textbf{(2)}$$

Where P is total applied load at each increment of displacement obtained from the experimental tests and a is the distance between the applied point load and support, $a = 800\ mm$.

In general, the flexural response of RC beam specimens strengthened with CFRP rods using the SNSM technique corresponded well to the flexural response of beams strengthened with CFRP rods using the NSM technique. This is also true regarding the ultimate strength capacity, specially with regard to beams BC2(210-SR) and BC3(270-SM).

Based on **Fig. 11-a**, Beams BC1(270-SR) and BC5(270-UR) exhibited flexural performance similar to that of beam S-C6(270-R) in the elastic and cracking phases; however, while different slopes of the moment deflection curves were observed after tensile steel yielding. This difference between slopes was attributed to the position of the CFRP rods, i.e. the SNSM-CFRP rods were closer to the neutral axis as a result of the implementation of the SNSM technique, and consequently, this led to reduce their carried tensile forces which means reduction in the increasing rate of the SNSM beam resisting moment. The maximum variation in the $(M-\delta)$ curves was recorded at the failure moment. Failure of beam S-C6(270-R) occurred at 53.3 kN.m; and this value is about 6.9 kN.m (14.9%) greater than that of beam BC1(270-SR), and about 12.2 kN.m (29.7%) greater than that of beam BC5(270-UR). Although the failure moments in beams BC1(270-SR) and BC5(270-UR) are smaller than the failure moment in beam S-C6(270-R) due to the position of the additional strengthening bars; the SNSM technique used in this case helped to prevent slippage of the CFRP rods out of the strengthening system. Applying the SNSM technique caused to change the failure mode from CFRP rods pull out in S-C6(270-R) to compressed concrete crushing in BC1(270-SR) and BC5(270-UR). **Fig. 12** compares the failure mechanism of beams BC1(270-SR) and BC5(270-UR) with that of beam S-C6(270-R).

Figure 11-b indicates that the $(M-\delta)$ curves corresponding to beams BC3(270-SM) and S-C6(270-M) are almost identical. The ultimate bending moment capacity of beam BC3(270-SM) was 1.5 kN.m (3.4%) less than that of beam S-C6(270-M). This great convergence between the both strength capacities, despite different locations of CFRP bars, might suggest that to the proposed SNSM technique has the capacity to put off the debonding failure occurrence. Indeed, the S-C6(270-M) beam was mainly failed due to debonding failure at the mortar–concrete interface before concrete crushing, whereas debonding failure was occurred simultaneous with the compressed concrete crushing in the BC3(270-SM) beam. **Fig.13** illustrates the debonding failure mechanism in the both beams (BC3(270-SM) and S-C6(270-M)).

Figure 11-c indicates that the ultimate capacity of beam S-C6(210-R) was 1.4kN.m (3.3%) higher than the ultimate capacity of beam BC2(210-SR). The S-C6(210-R) and BC2(210-SR) beams were both failed due to concrete peeling off at the end of the CFRP rods. This result confirms that, the peeling off failure is attributed more to the strengthening length than to the strengthening technique used (NSM or SMSM). The strengthening length (SL) to the beam length (BL) ratio of this set of beams $(\frac{SL}{BL}=0.56)$ is consistent with the expected peeling off failure ratio suggested in [**10**]. However, **Fig. 14** illustrates the peeling off failure mechanism of beams S-C6(210-R) and BC2(210-SR).

Regarding the displacement ductility, it is worth noting that beams strengthened with CFRP rods using the SNSM technique proved to be more ductile as compared to the NSM beams, except for BC2(210-SR) for which the ductility index remained the same as that of beam S-

C6(210-R). The overall improvement in ductility of SNSM beams is most likely referred to the failure mode and the interaction between the additional reinforcement location and the tension steel deformation. **Fig. 15** gives a comparison between the ductility indices ($\boldsymbol{\mu}$) of SNSM and NSM beams.

5 Analytical model- Application of conventional prediction techniques

5.1 Prediction of deflection response ($(\delta)_{\text{mid}}$)

The American Concrete Institute ACI 318-08 [26] recommendations were employed in calculating the short-term deflection of reinforced concrete beams strengthened with CFRP rods using the SNSM technique under service loads. The mid-span deflections of beams could be computed as a function of the bending moment (*M=(P/2).a*) as expressed in Eq.(3). Hence, the center deflections corresponding to the cracking, yielding and ultimate moment of beams were obtained in this study according to the sequence presented in **Fig. 16.**

$$(\delta)_{\text{mid}} = \frac{M}{24\ \mathrm{E_c I}_{eff}}(3\mathrm{L}^2 - 4\mathrm{a}^2) \tag{3}$$

Where, $\mathrm{E_c}$ is the elastic modulus of concrete ($\mathrm{E_c} = 4700\sqrt{f_c'}$) and I_{eff} is the effective moment of inertia of the entire beam. The effective moment of inertia suggested by Branson was adopted and can be determined as follows [26,29]:

$$I_{eff} = (\frac{M_{cr}}{M_a})^3\ I_g + \left[1 - \left(\frac{M_{cr}}{M_a}\right)^3\right] I_{cr} \leq I_g \tag{4}$$

Where, M_a is the maximum moment calculated at the point of deflection of the beam, I_g is the gross moment of inertia, I_{cr} is the cracked moment of inertia and M_{cr} is the cracking moment.

The moment of inertia, I_{cr} of the cracked section is computed by assuming that the material has a linear elastic behavior, while neglecting the concrete below the neutral axis, as depicted in **Fig. 17**. Therefore, the position of the neutral axis (x) and the moment of inertia of the cracked section were computed using Eq.(5) and Eq.(6), respectively.

$$\boldsymbol{x} = \frac{-[\boldsymbol{nA_{s+}n_fA_f}] \mp \sqrt{[\boldsymbol{nA_s} + \boldsymbol{n_fA_f}]^2 + 4\frac{\boldsymbol{b}}{\boldsymbol{2}}\ [\boldsymbol{n_fA_fd_f} + \boldsymbol{nA_sd_s}]}}{\boldsymbol{b}} \tag{5}$$

$$\boldsymbol{I_{cr}} = \frac{\boldsymbol{bx^3}}{\boldsymbol{3}} + \boldsymbol{nA_S(d_s - x)^2} + \boldsymbol{n_fA_f(d_f - x)^2} \tag{6}$$

Where, $n = \frac{E_s}{E_c}$, $n_f = \frac{E_f}{E_c}$, b is the width of the cross section, A_S is the area of tension steel, A_f is the area of SNSM CFRP bars, $d_s$is the effective depth of steel bars and d_f is the effective depth of the CFRP rods.

In fact, applying Eqs.(5) and (6), for deflection calculations (Eq.(3)), when $M_a \gg M_{cr}$ (i.e. I_{eff} equals to I_{cr}) was found to underestimate the deflection in the SNSM-CFRP beams. For this reason, the moment of inertia, I_{cr} was computed again while neglecting the elastic modulus of the steel reinforcement in the stage of $\boldsymbol{\delta(M_u - M_y)}$ only, **Fig. 16**. This slight modification could be justified by following:

- The additional resistance of the strengthened beams to the external applied load in the ultimate strength phase (from the steel yielding load to failure load) was basically induced due to the presence of CFRP rods [6]. This can be seen in **Fig. 4** (**section 3.1**) where all the strengthened beams showed load increasing rates greater than that of the control beam.
- The SNSM reinforcing bars start controlling the propagation of cracks in the strengthened beams once the tensile stress in the steel reinforcement exceeded the yielding point [21].

5.2 Prediction of cracking moment(M_{cr})

The predicted cracking moment ($M_{cr} = {f_t I_{tr}}/{y_b}$) of the SNSM-CFRP beams was calculated by assuming that concrete fibers in the tension zone had reached their maximum tensile stress ($\sigma = f_t$). Where f_t is the concrete tensile strength, I_{tr} is the un-cracked moment of inertia of the transformed section (**see appendix A**) and y_b is the distance between the most tensile concrete fiber and the neutral axis before cracking.

5.3 Prediction of yielding moment(M_y)

In the same way of cracking moment, the predicted yielding moment ($M_y = {f_y I_{cr}}/{ny}$) was calculated by assuming that the tension steel reinforcement had achieved the elastic behavior ($\sigma = f_y$). Where f_y is the elastic limit stress of the tensile steel and ($y = d_s - x$) is the distance between the steel bars and the neutral axis.

5.4 Prediction of ultimate moment(M_u)

The ultimate moment of SNSM strengthened beam is assessed by the force equilibrium conditions and the stress-strain relation of concrete in compression and steel reinforcement in tension [15], as presented in (**appendix B**). The assumption includes: (1) Conventional flexural failure of strengthened beam; i.e. crushing of the compressed concrete after yielding of the tension steel reinforcement. (2) Perfect bond between the internal surface of concrete and the filling material (resin or mortar). (3) The tensile strength of concrete is totally neglected. (4) The stress-strain relation of the concrete and steel suggested by ACI-318-08 is adopted.

. .

5.5 Performance of the analytical model.

Figure 18 compares the calculated deflections of the tested RC beams at the cracking, yielding and ultimate levels with the experimental results. Overall, the analytical model gave quite a good estimation of the experiment deflections in beams strengthened with SNSM-CFRP bars. The ratio of the computed ultimate deflection to the experimental deflection ($(\delta)_{u\ (calculated)}/(\delta)_{u\ (experimental).}$) are approximately 0.87, 0.88, 1.15, 1.24 and 1.06 for beams BC1(270-SR), BC2(210-SR), BC3(270-SM), BC4(210-SM) and BC5(270-UR), respectively.

Moreover, **Fig. 19** shows a comparison between the experimental and the predicted bending moment-deflection relationships for the SNSM-CFRP beams. The bending moments obtained from the above analytical model and the experimental values were found to be in good agreement. The ratio of the $M_{u\ (calculated)}$ to the $M_{u\ (experimental)}$ are 1.03, 1.12, 1.13, 1.27 and 1.07 for beams BC1(270-SR), BC2(210-SR), BC3(270-SM), BC4(210-SM) and BC5(270-UR), respectively.

The significant overestimated ultimate values in beam BC4(210-SM) (1.24 for deflection and 1.27 for moment) were primarily due to the early debonding failure which is not considered in the current analytical model. Further analytical studies to include such failures are strongly recommended.

6 Conclusion:

The present study aimed to analyze the global flexural response of RC beams strengthened with CFRP rods using the SNSM technique. The experimental results obtained and the studies conducted allowed drawing the following conclusions:

- The Side Near Surface Mounted (SNSM) technique helped to improve the global flexural performance of RC beams whatever the strengthening scenario used. The load-bearing capacity of the beams BC1(270-SR), BC2(210-SR), BC3(270-SM),BC4(210-SM) and BC5(270-UR) were greater than that of the control beam by 59.3%, 46.2%, 45.6%, 29.3% and 41.1%, respectively.
- CFRP rods placed laterally adjacent to the steel bars and embedded in resin formed better resisting action to the flexural bending than those embedded in mortar or placed upper than the main tension steel. In BC1(270-SR) beam, the flexural strength increased over 59% compared to the control beam without large loss in ductility.
- The length of CFRP rods was found to have a considerable influence on the failure mode and energy absorption capacity. Two strengthened beams, i.e. BC2(210-SR) and BC4(210-SM), out of five beams showed premature failure due to the insufficient strengthening length (210 cm). The ratio of the strengthening length *SL* to the beam length *BL* of the both beams was about 0.56. However, using mortar caused the failure mode to change from peeling-off failure in BC2(210-SR) to early debonding failure in BC4(210-SM).

- The strengthening position did not display significant impact on the failure mode. Beams BC1(270-SR) and BC5(270-UR) were both failed due to concrete crushing. However, the failure mode of beam BC3(270-SM) was debonding failure at the interface concrete–mortar because of the mortar filling material.
- According to the experimental data provided by this investigation; the Side Near Surface Mounted (SNSM) strengthening system can be used as an alternative to the Near Surface Mounted (NSM) system; it can in some cases help to avoid the non-conventional failure modes (pull-out of CFRP rods or early debonding failure). Furthermore, the SNSM-CFRP beams showed higher ductility behavior as compared to the NSM-CFRP beams.
- The computed flexural strength capacity and mid-span deflection of the strengthened beams, using the conventional prediction models, showed excellent agreement with the experimental results.

Acknowledgement

The authors acknowledge the financial support of the Freyssinet Company, France.

Appendix (A): Calculation of the transformed moment of inertia.

The moment of inertia of the transformed section of the beam strengthened with SNSM-CFRP rods was calculated based on Eq. (A.1).

$$I_{tr} = \frac{by_{nc}^3}{3} + \frac{b(h-y_{nc})^3}{3} + (n-1)A_S(d_s - y_{nc})^2 + \left(n_f - 1\right)A_f\left(d_f - y_{nc}\right)^2 \quad \textbf{(A.1)}$$

Where y_{nc} is the neutral axis depth of the transformed section; it was calculated by equating the sum of areas above and below the neutral axis as given in Eq. (A.2):

$$y_{nc} = \frac{\frac{bh^2}{2} + nA_S d_s - A_S d_s + n_f A_f d_f - A_f d_f}{bh + nA_S - A_S + n_f A_f - A_f} \quad \textbf{(A.2)}$$

Appendix (B): Calculation of the failure moment.

The ultimate resisting moment (M_u) of the SNSM-CFRP bars strengthened beam was assessed by applying the equilibrium conditions ($C = F_s + F_f$) and the stress-strain correlation requirements, as presented in **Fig. B1**, where C, F_s and F_f are the compressive force, tensile steel force and tensile CFRP force, respectively.

The neutral axis location in a beam section where failure occurs can be computed as given below:

$$k_1 c^2 + k_2 c + k_3 = 0 \quad \textbf{(B.1)}$$

$$k_1 = 0.85 f_c' \mathrm{b} \beta \quad \textbf{(B.2)}$$

$$k_2 = -(A_S f_y - \varepsilon_{cu} A_f E_f) \quad \textbf{(B.3)}$$

$$k_3 = -(A_f E_f \varepsilon_{cu} d_f) \quad \textbf{(B.4)}$$

$$c = \frac{-k_2 \mp \sqrt{k_2^2 - 4k_1 k_3}}{2k_1} \quad \textbf{(B.5)}$$

The ultimate compressive strain ε_{cu} in concrete was assumed equal to 0.003, based on the compressive test results; this value is similar to the one suggested by the ACI 318-08 Building Code. However, the maximum strain of CFRP rods, corresponding to the failure load, was evaluated using similar triangles as follows:

$$\varepsilon_f = \frac{\varepsilon_{cu}}{c} d_f - \varepsilon_{cu} \quad \textbf{(B.6)}$$

Therefore, the ultimate moment of the SNSM-CFRP section can be expressed using the following formula:

$$M_u = A_S f_y \left(d_s - \frac{\beta c}{2} \right) + \varepsilon_f A_f E_f (d_f - \frac{\beta c}{2}) \quad \textbf{(B.7)}$$

References

[1] L. Lam and J. G. Teng. Strength Models for Fiber-Reinforced Plastic-Confined Concrete. Journal of Structural Engineering 2002; 128(5).

[2] L.J. Li , Y.C. Guo, F. Liu, J.H. Bungey. An experimental and numerical study of the effects of thickness and length of CFRP on performance of repaired reinforced concrete beams. Construct Build Mater 2006;20(10):901–9

[3] M. Onal Mustafa. Strengthening reinforced concrete beams with CFRP and GFRP. Adv Mater Sci Eng 2014:1–8.

[4] A.N. Nayak, A. Kumaria , R.B. Swainb. Strengthening of RC Beams Using Externally Bonded Fibre Reinforced Polymer Composites Structures 2018;14: 137–152.

[5] S.S. Zhang, T. Yu ,G.M. Chen . Reinforced concrete beams strengthened in flexure with near-surface mounted (NSM) CFRP strips: Current status and research needs, Composites Part B 2017,131: 30-42

[6] F. Al-Mahmoud, A. Castel, R. François, C. Tourneur. Strengthening of RC members with near-surface mounted CFRP rods. Composite Structures 2009; 91:138-147

[7] T. Hassan, S. Rizkalla. Investigation of bond in concrete structures strengthened with near surface mounted carbon fiber reinforced polymer strips. J Compos Constr., 2003; 7(3):248–57

[8] J.A. Barros, D.R. Ferreira, A.S. Fortes, S.J. Dias. Assessing the effectiveness of embedding CFRP laminates in the near surface for structural strengthening. Constr. Build Mater 2006; 20(7):478–91.

[9] L. De Lorenzis, and J.G. Teng. Near-surface mounted FRP reinforcement: an emerging technique for strengthening structures. Composites Part B-Engineering 2007; 38(2):119-143.

[10] F. Al-Mahmoud, A. Castel, R. François. Failure modes and failure mechanisms of RC members strengthened by NSM CFRP composites – Analysis of pull-out failure mode. Composites Part B 2012; 43: 1893-1901.

[11] A. Kreit , F. Al-Mahmoud , A. Castel , R. François . Repairing corroded RC beam with near surface mounted CFRP rods. Mater Struct. 2011; 44(7):1205–17.

[12] I.A. Sharaky, L. Torres, J. Comas, C. Barris. Flexural response of reinforced concrete (RC) beams strengthened with near surface mounted (NSM) fibre reinforced polymer (FRP) bars, Compos. Struct. 2014;109: 8–22.

[13] A. M. Khalifa. Flexural performance of RC beams strengthened with near surface mounted CFRP strips Alexandria Engineering Journal 2016; 55: 1497–1505

[14] W.M. Sebastian and J. Vincent, S. Starkey. Experimental characterisation of load responses to failure of a RC frame and a NSM CFRP RC frame. Construction and Building Materials 2013; 49: 962–973.

[15] ACI. Guide for the design and construction of externally bonded FRP systems for strengthening concrete structures. American Concrete Institute, ACI 440.2R-08, Farmington Hills,2008.

[16] L. De Lorenzis , and A. Nanni. Characterization of FRP Rods as Near Surface Mounted Reinforcement,"Journal of Composites for Construction, ASCE 2001, V. 5, No. 2,pp. 114-121.

[17] B. Almassri, A. Kreit, F. Al Mahmoud and R. François Mechanical behaviour of corroded RC beams strengthened by NSM CFRP rods Composites: Part B 2014; 64: 97–107.

[18] L. De Lorenzis , F. Micelli , A. La Tegola . Passive and active near surface mounted FRP rods for flexural strengthening of RC beams. Proceeding of ICCI 02, San Francisco, 10-12 June 2002.

[19] L. De Lorenzis , A. Nanni . Bond between near-surface mounted fiber-reinforced polymer rods and concrete in structural strengthening. ACI Struct. J. 2002;99(2):123-132.

[20] L. De Lorenzis , A. Nanni , A. La Tegola . Flexural and shear strengthening of reinforced concrete structures with near surface mounted FRP rods. Proceeding of the 4th international Conference on Advanced Composites Materials in Bridges and Structures. (ACMBS) Ottawa 2000:521–8.

[21] Md Akter Hosen, Mohd Zamin Jumaat , A.B.M. Saiful Islam. Side Near Surface Mounted (SNSM) technique for flexural enhancement of RC beams. Materials & Design 2015; 83 : 587–597

[22] F. Al-Mahmoud , A. Castel , R. François , C. Tourneur . Effect of surface preconditioning on bond of carbon fiber reinforced polymer rods to concrete. Cem.Concr. Compos. 2007;29(9):677–89.

[23]M. Nadim Hassoun, A. Al-Manaseer, Structural Concrete: Theory and Design. John Wiley & Sons, 2012.

[24] F. Al-Mahmoud , A. Castel , R. François , C. Tourneur Anchorage and tension-stiffening effect between near-surface-mounted CFRP rods and concrete, Cement & Concrete Composites 33 (2011) 346–352.

[25] P.Mukhopadhyaya, R.N. Swamy, C. Lynsdale. Optimizing structural response of beams strengthened with GFRP plates. J Compos Construct, ASCE 1998;2(2):87–95.

[26] ACI. Building code requirements for reinforced concrete. American Concrete Institute, ACI 318, Farmington Hills, Michigan; 2008.

[27] A.A. Maghsoudi, H. Akbarzadeh. Flexural ductility of HSC members. Struct. Eng. Mech. 2006;24(2).

[28] V.S. Gopalaratnam, R. Gettu, On the characterization of flexural toughness in fiber reinforced concretes, Cement Concr. Compos. 17 (3) (1995) 239–254.

[29] D.E. BRANSON, Instantaneous and Time-Dependent Deflections of Simple and Continuous Reinforced Concrete Beams, HPR Report No. 7, Part 1, Alabama Highway Department, Bureau of Public Roads, Alabama, 1965.

Figures

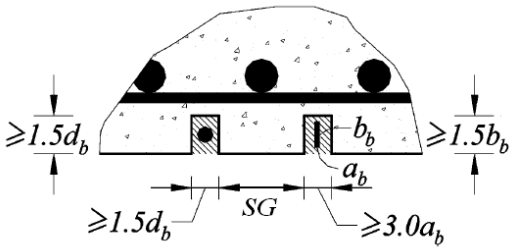

Fig. 1. Minimum dimensions of grooves

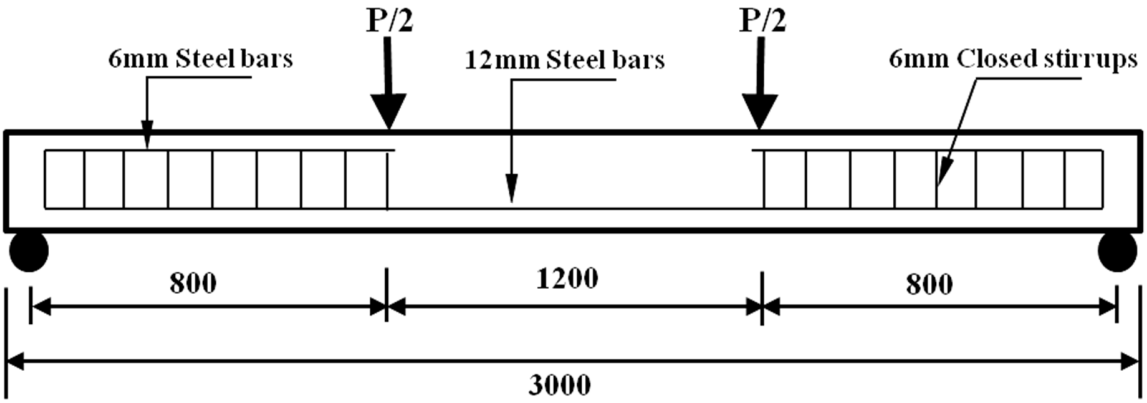

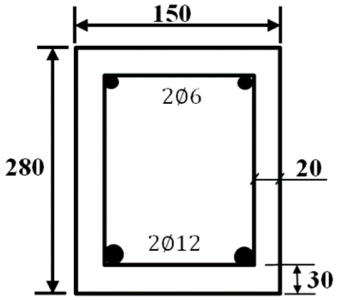

Beam cross-section before strengthening. (CB)

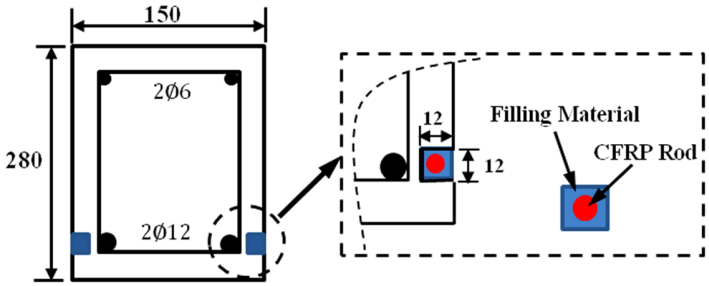

Beam cross-section after strengthening with CFRP rods by using the SNSM technique.(BC1-BC4)

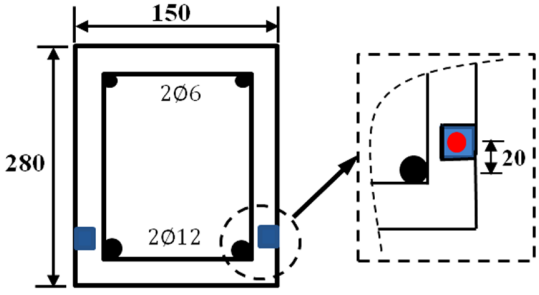

Beam cross-section after strengthening with CFRP rods by using the SNSM technique.(BC5)

Fig. 2. Test beams details and reinforcement configuration. (All dimensions in mm)

(a)

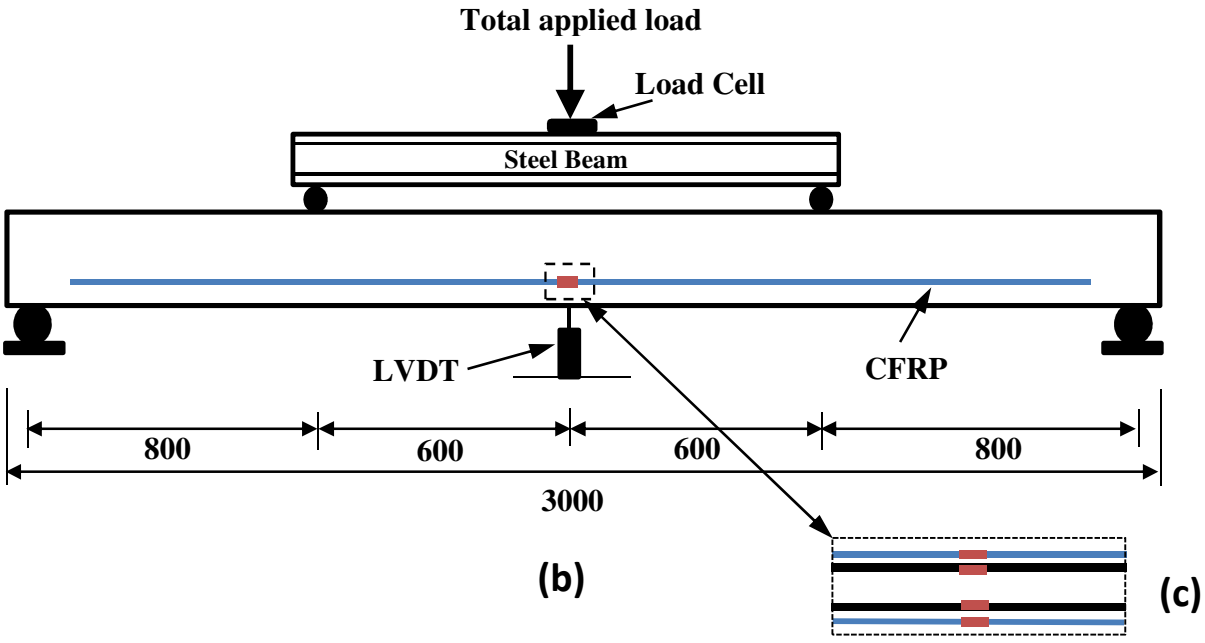

Fig. 3. (a) Test setup, (b) Instrumentation and (c) Strain gauges of steel and CFRP bars(top view). (All dimension in mm)

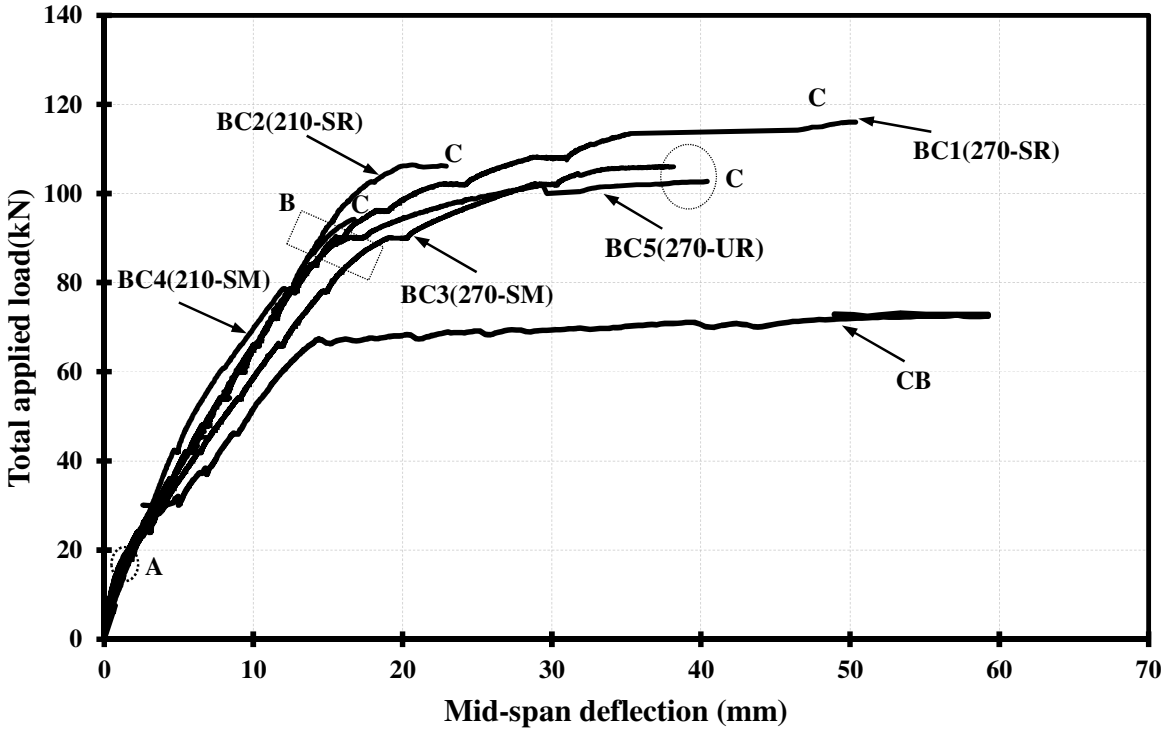

Fig. 4. Load vs. mid-span deflection curves

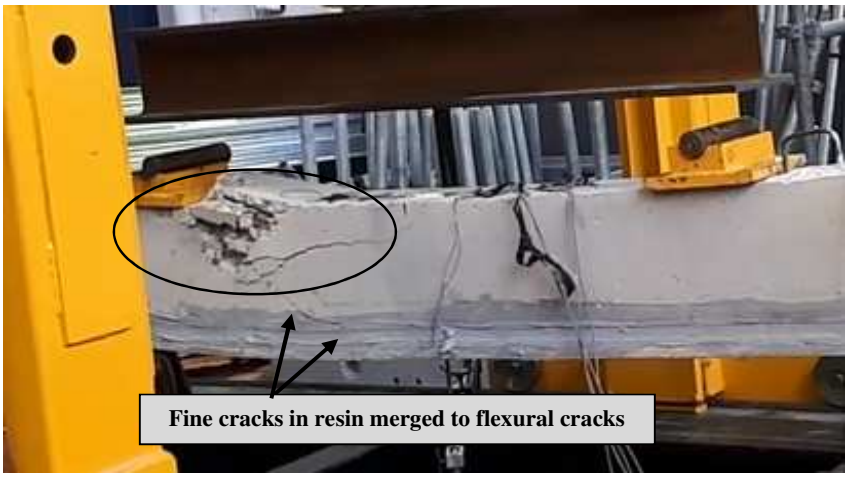

(a)

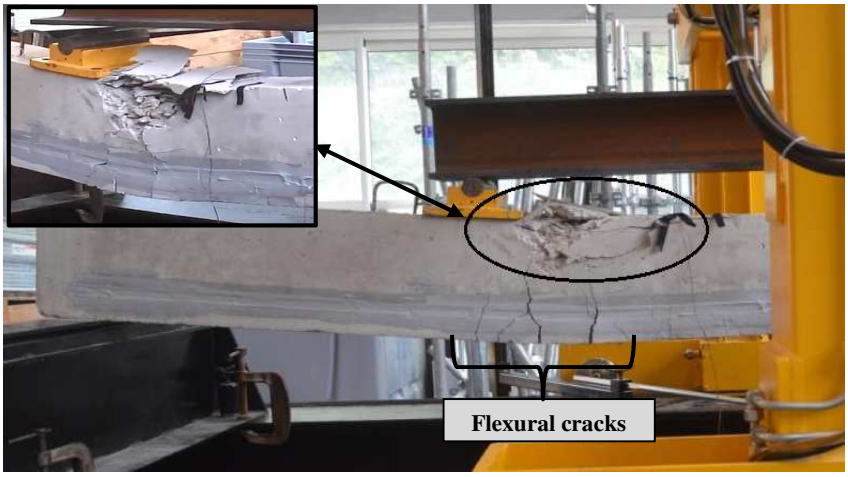

(b)

Fig. 5. Failure mode of beams; (a) BC1(270-SR) and (b) BC5(270-UR)

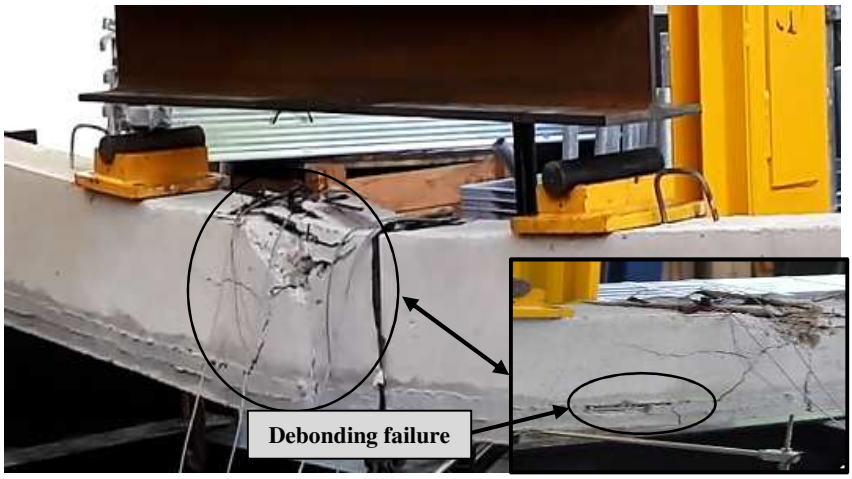

(a)

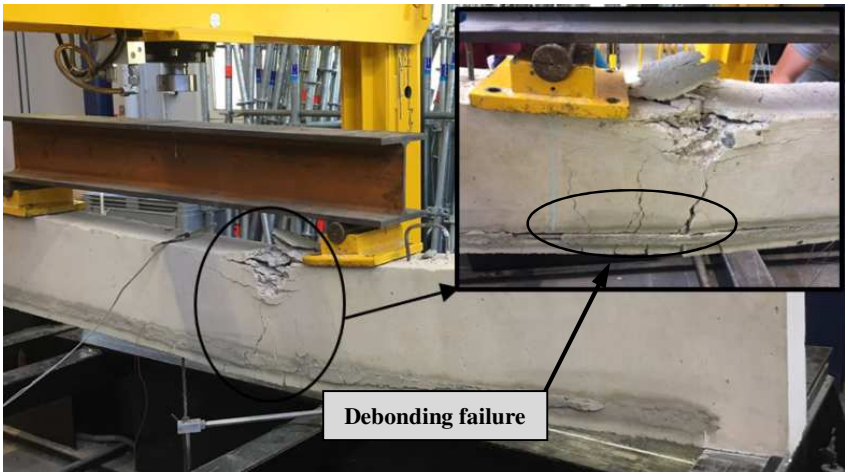

(b)

Fig. 6. Failure mode of beams: (a) BC3(270-SM) and (b) BC4(210-SM)

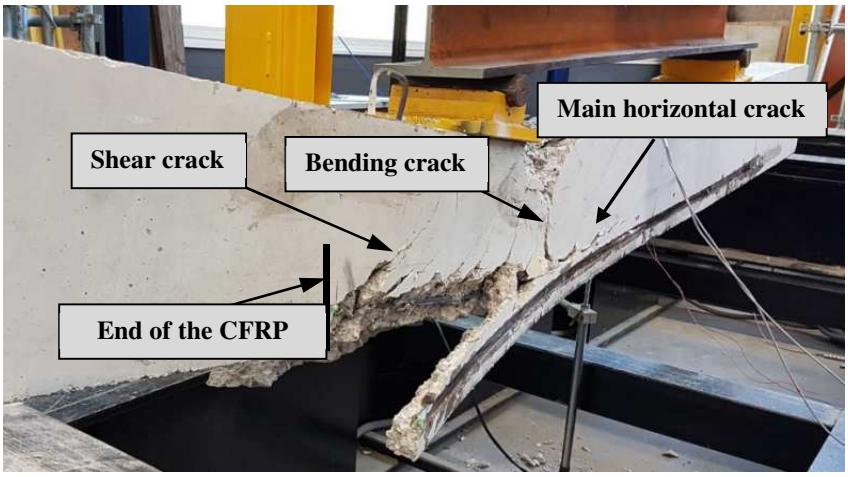

Fig. 7. Failure mode of beam: BC2(210-SR)

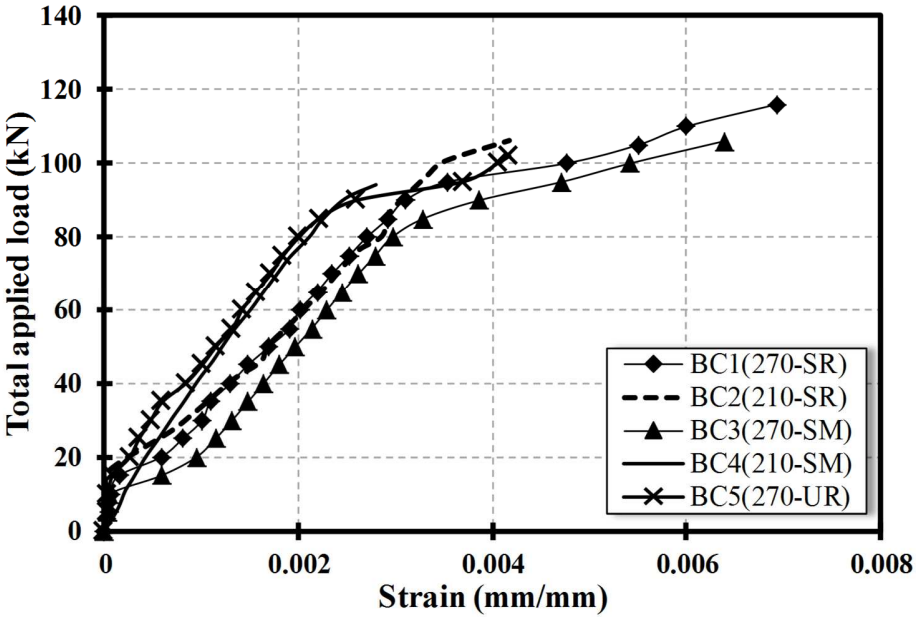

Fig. 8. Total applied load vs. strains of the CFRP rods

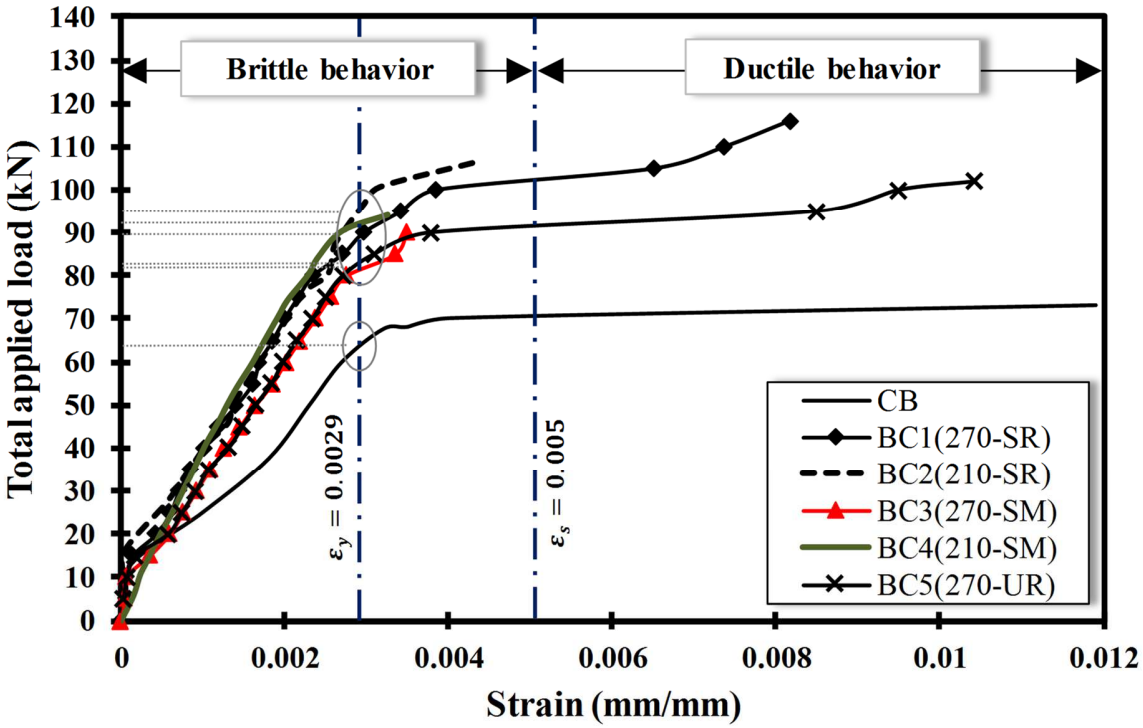

Fig. 9. Total applied load vs. steel strain

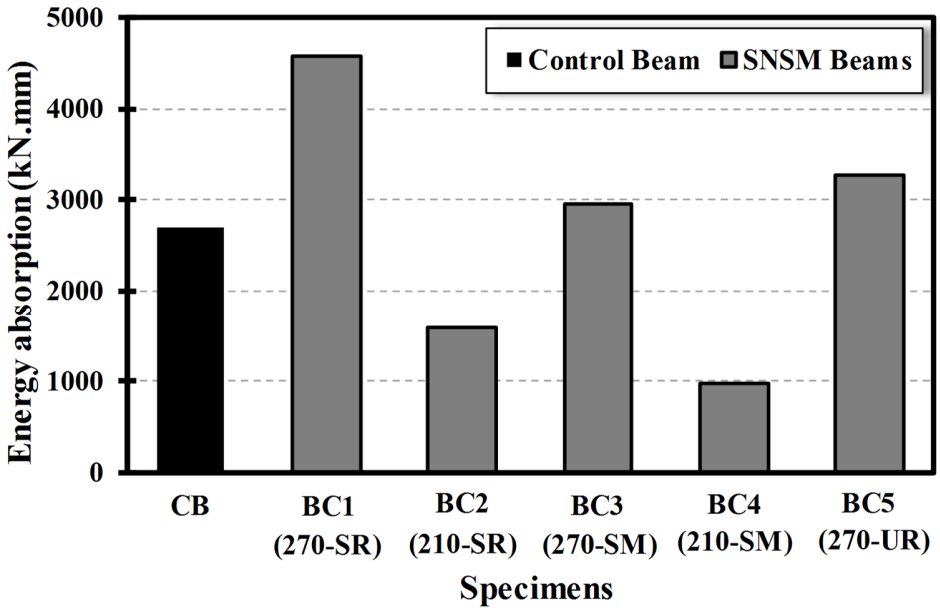

Fig.10 Energy absorption of beam speicemns

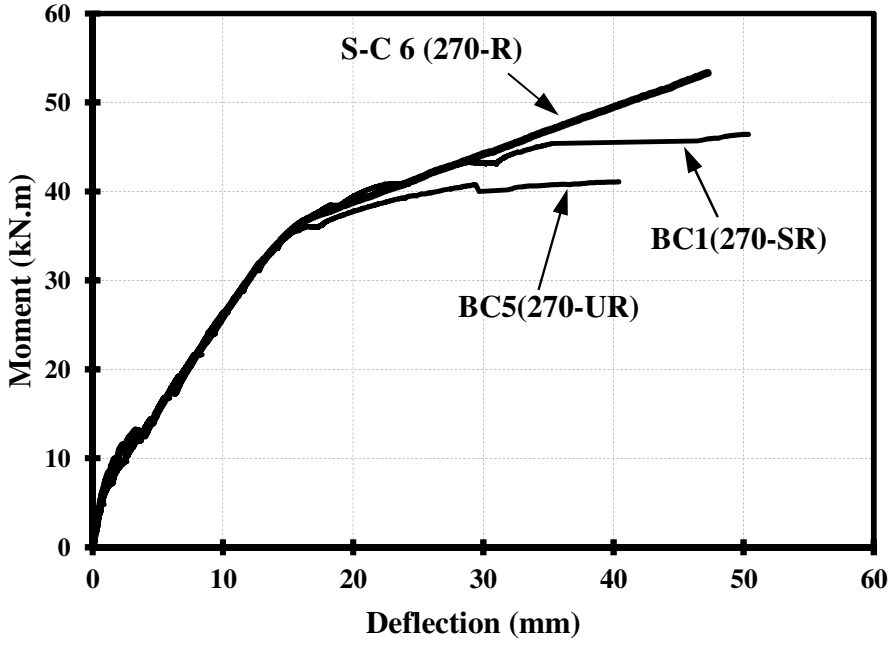

a) S-C6(270-R) vs. (BC1(270-SR) & BC5(270-UR)

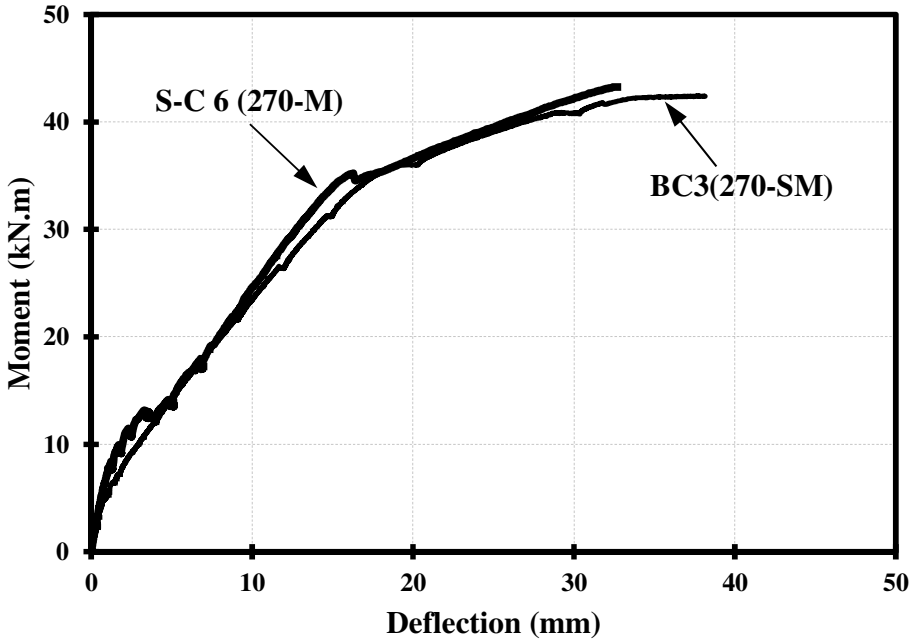

b) S-C6(270-M) vs. BC3(270-SM)

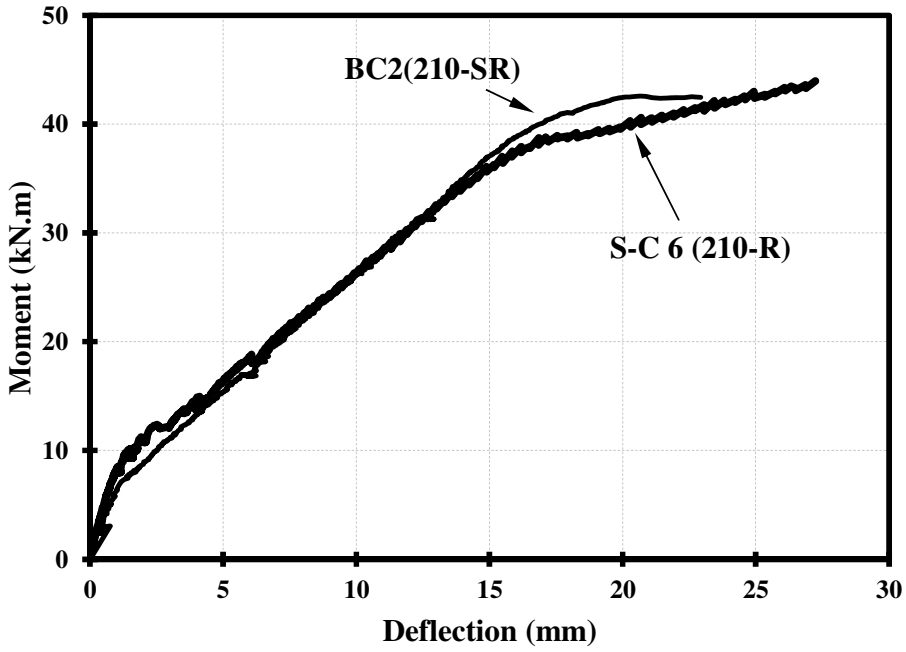

c) S-C6(210-R) vs. BC2(210-SR)

Fig. 11. SNSM vs. NSM moment-deflection curve

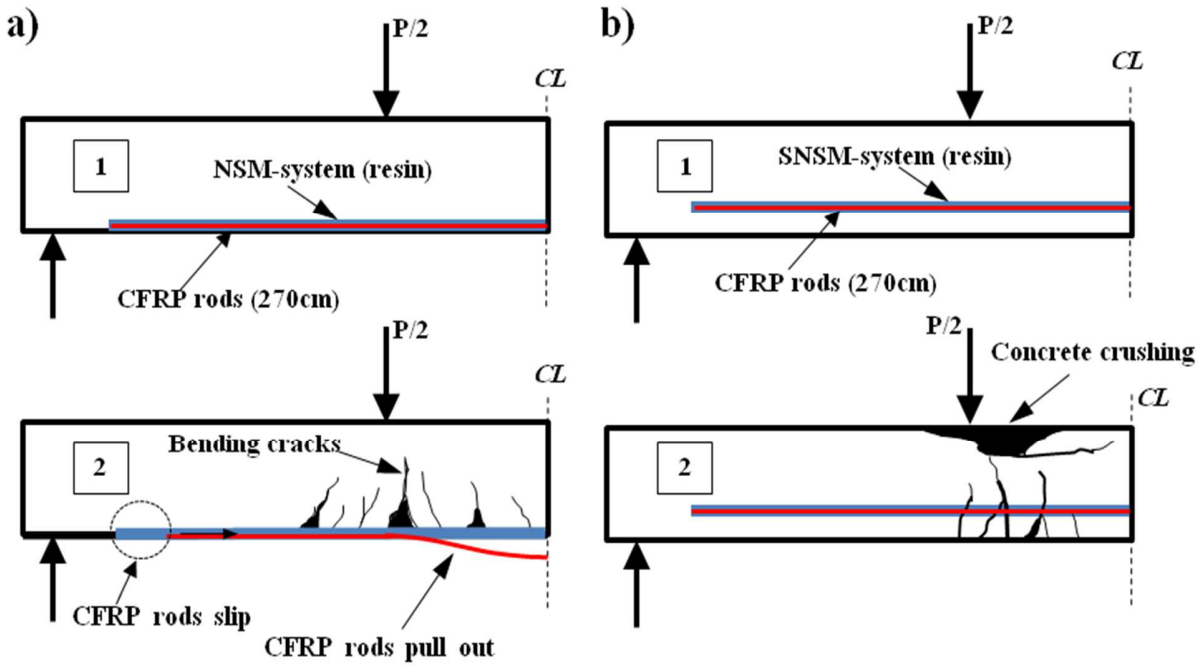

Fig. 12. Failure mechanism of a) S-C6(270-R) beam and b) BC1(270-SR) and BC5(270-UR) beams.

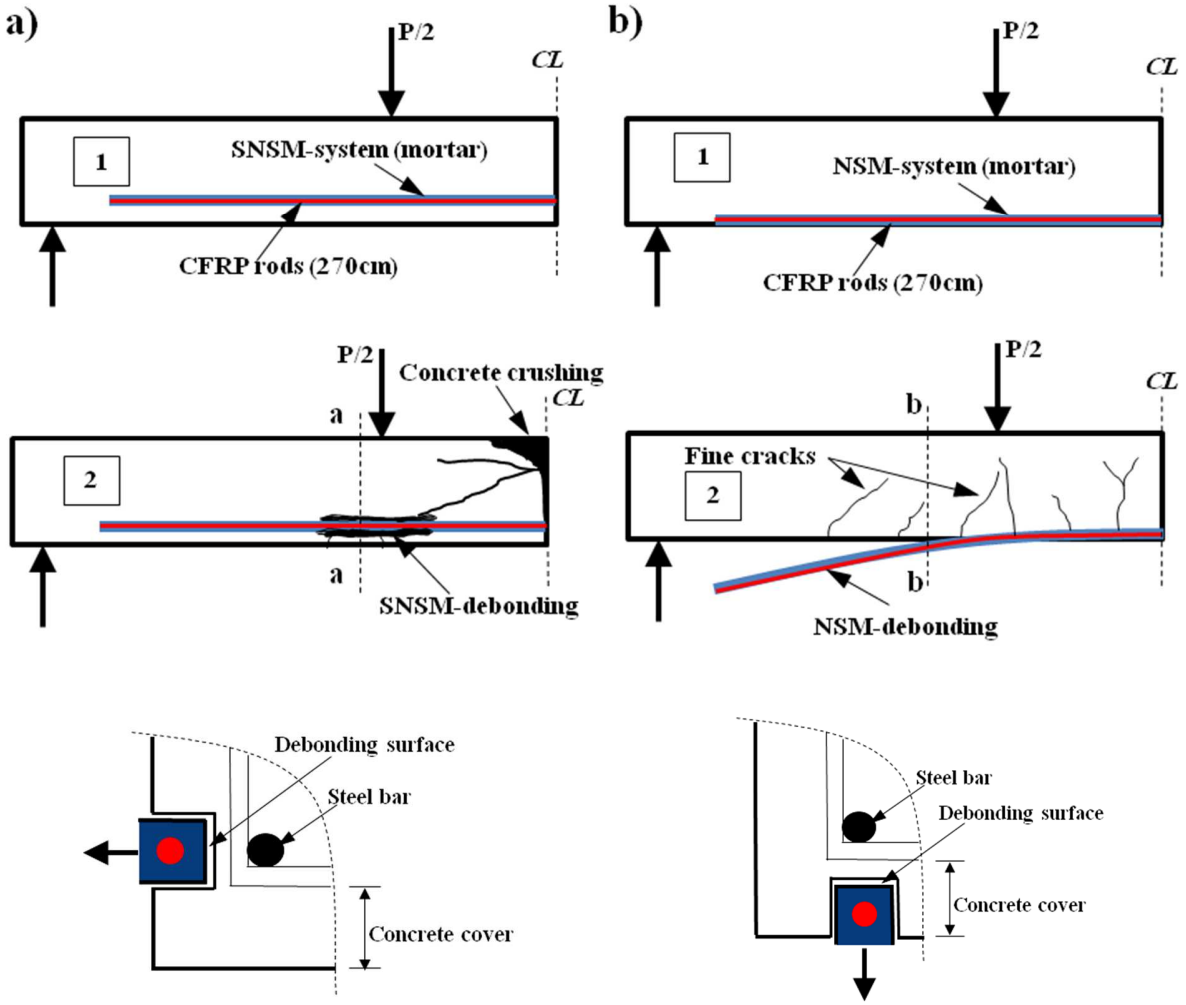

Fig. 13. Debonding failure mechanism of : a) BC3(270-SM) beam and b) S-C6(270-M) beam

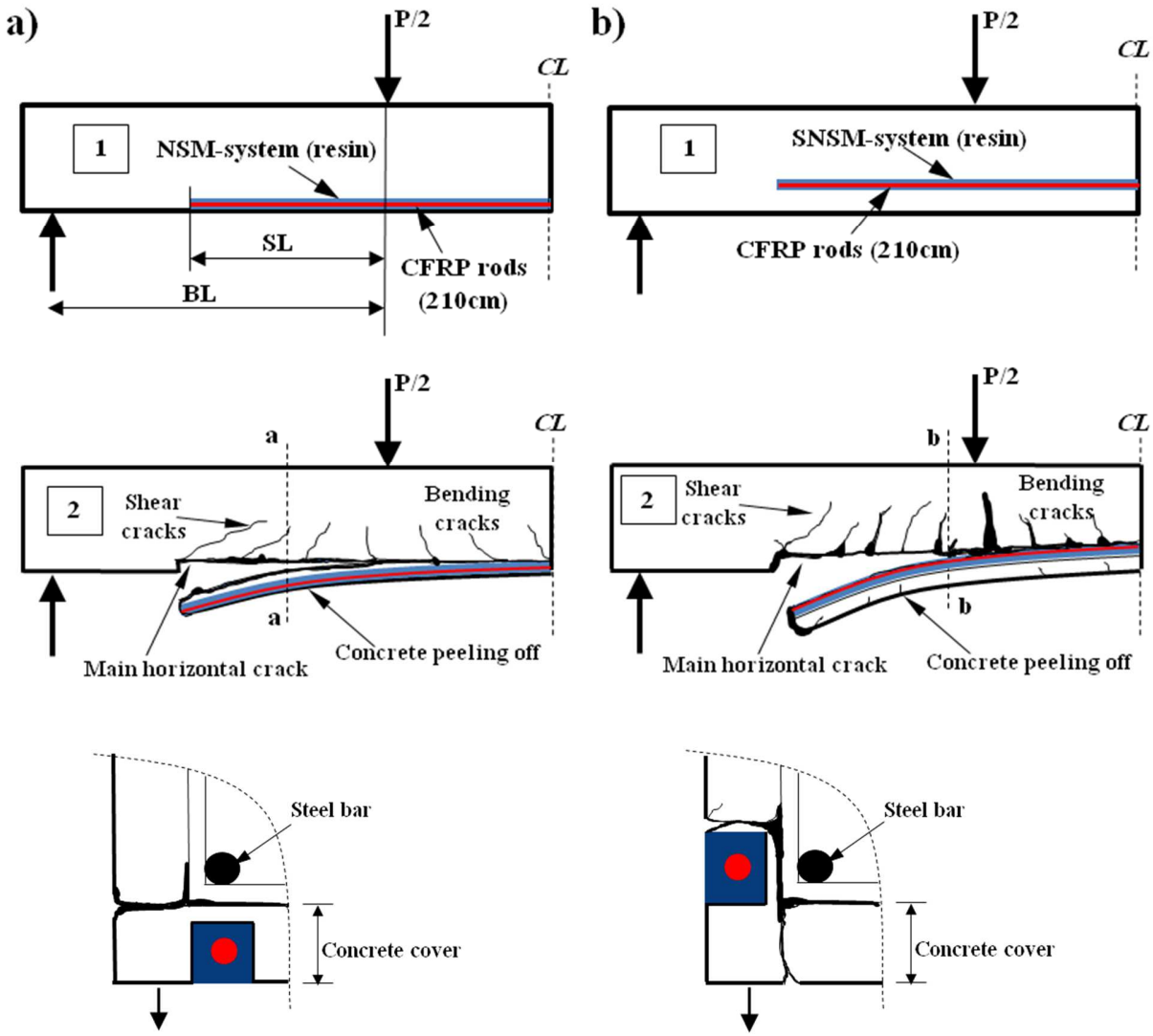

Fig. 14. Peeling off failure mechanism of: a) BC2(210-SR) beam and b) S-C6(210-R) beam

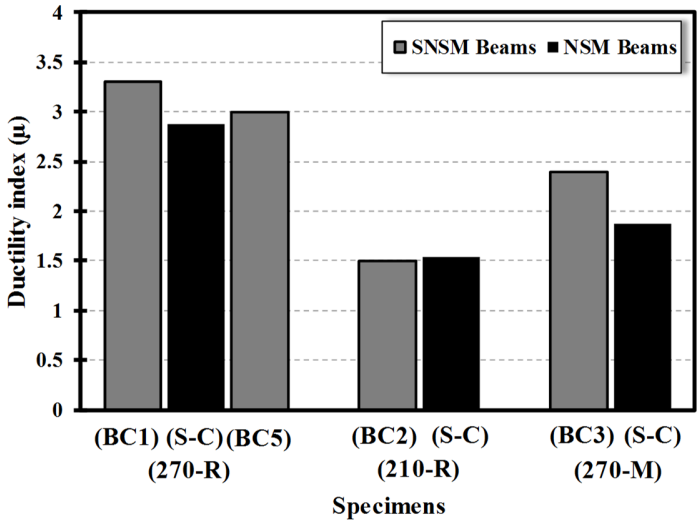

Fig. 15. Ductility comparison between the SNSM and NSM specimens

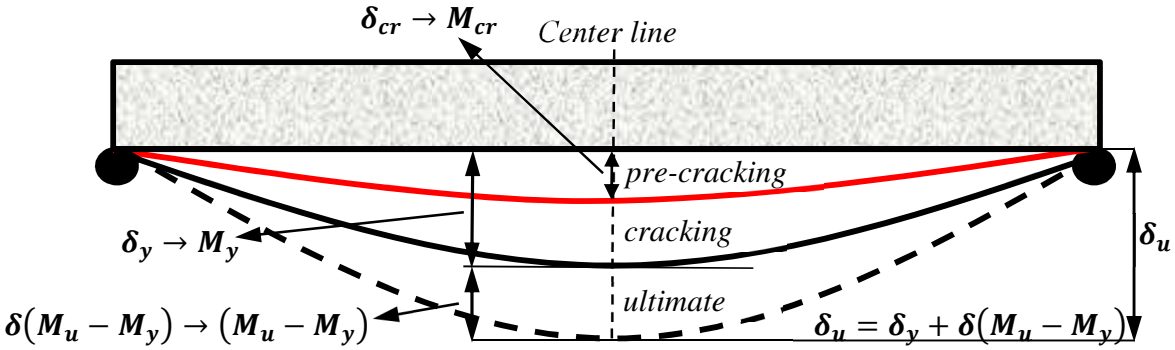

Fig. 16. Deflection calculation methodology

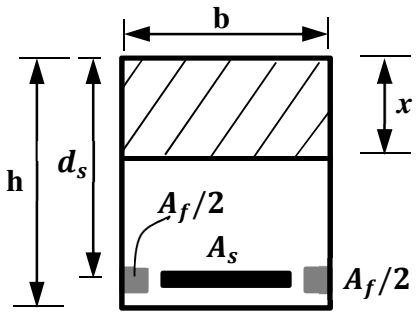

Fig. 17. Cracked section

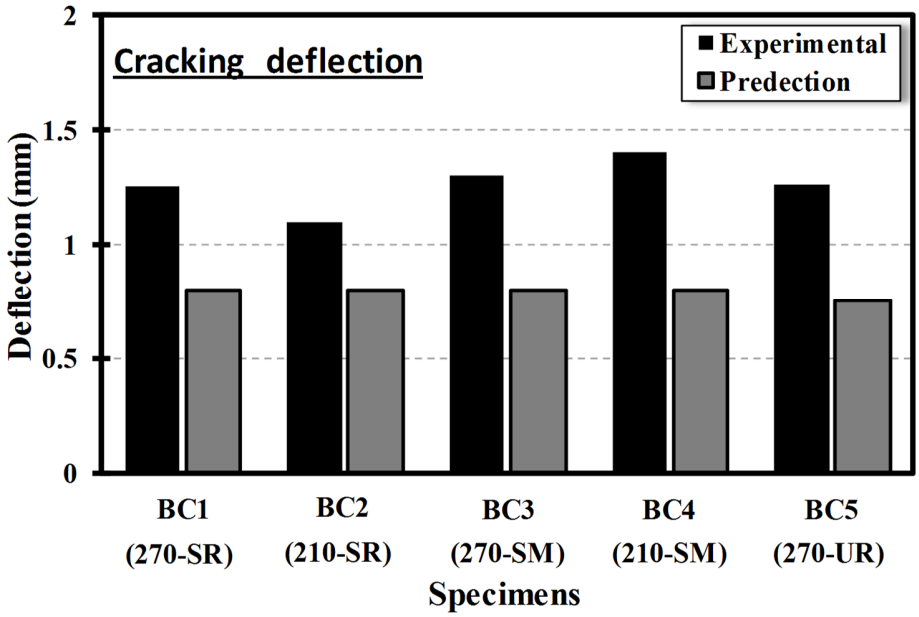

\

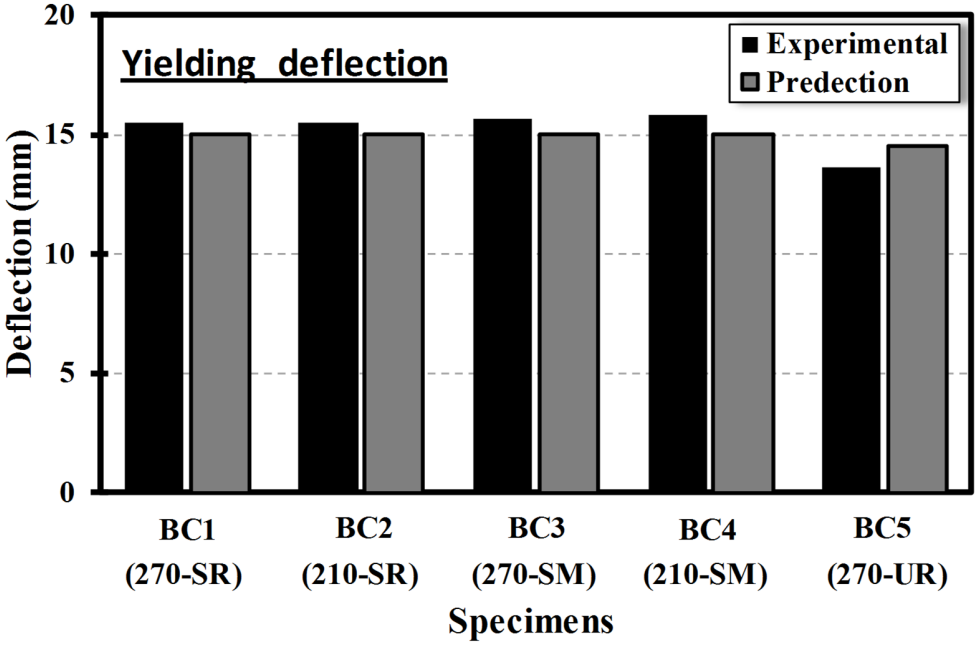

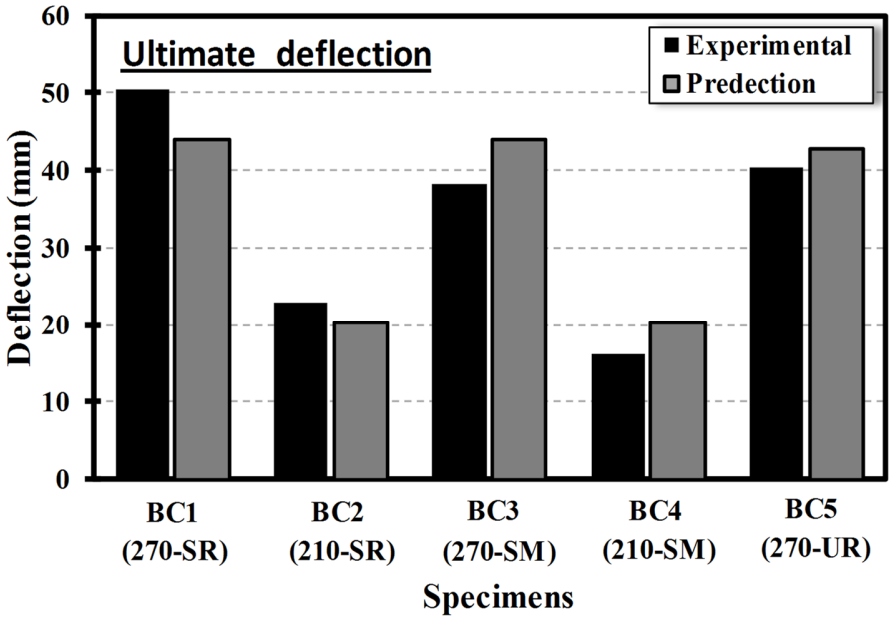

Fig. 18. Compression between the experimental and computed deflection.

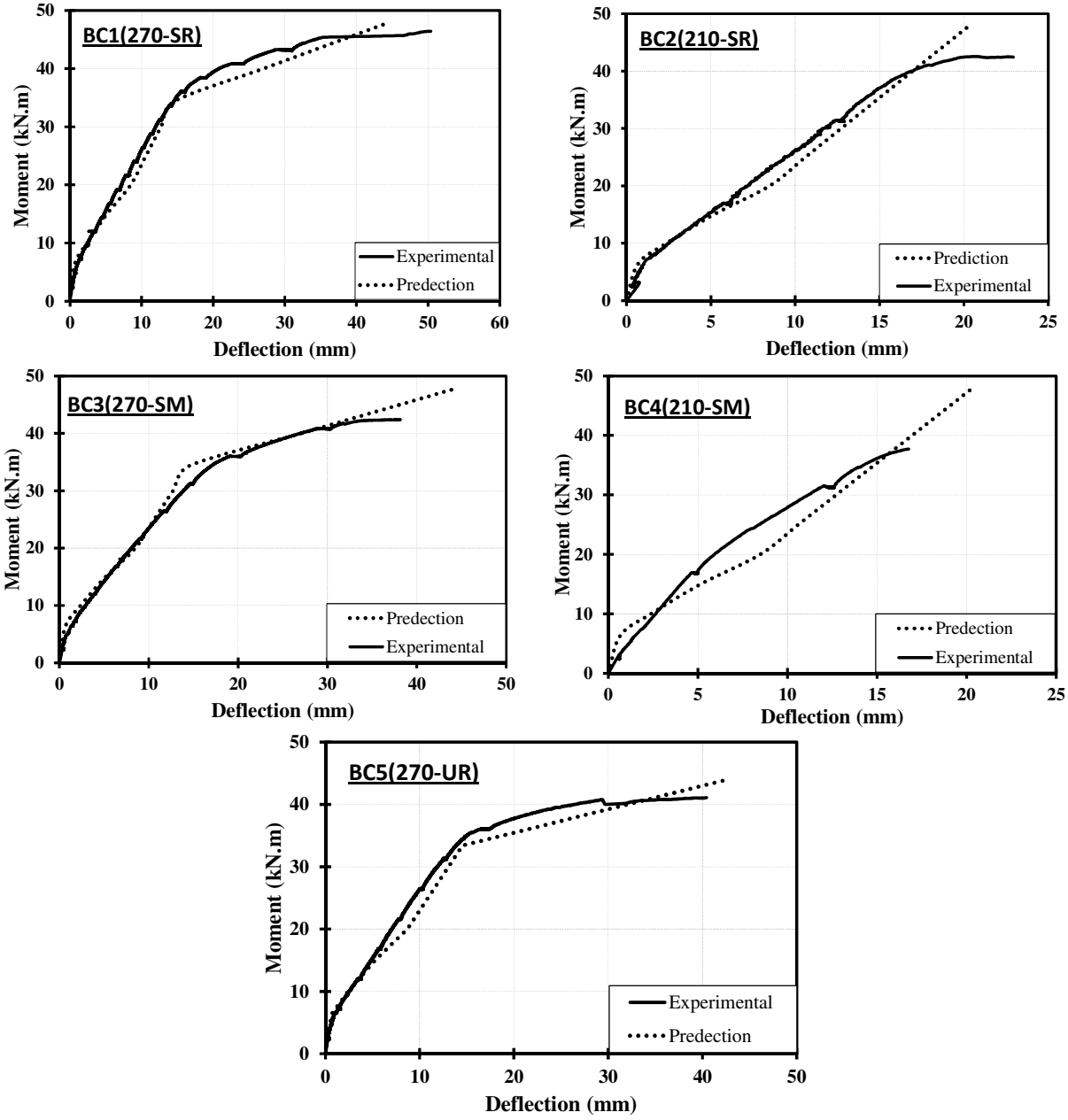

Fig. 19. Comparison between experimental and theoretical moment-deflection curves

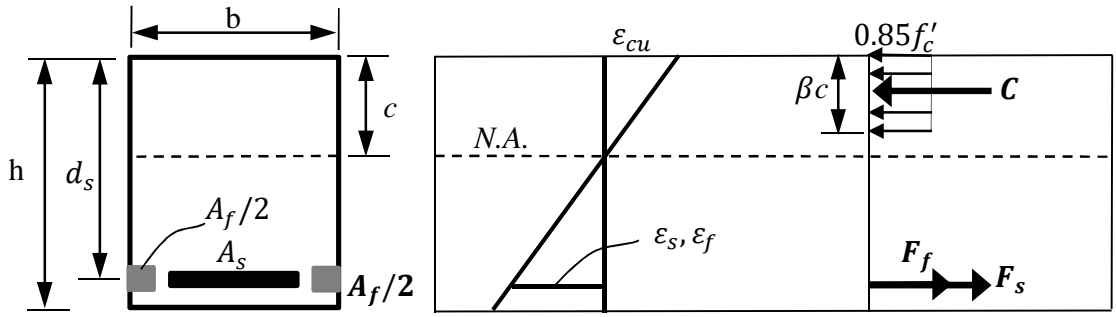

Fig. B1. Strain, stress and forces of the cross section

Tables

Table 1 Characteristics of the filling material

Material	Compressive strength (MPa)	Tensile strength (MPa)
Epoxy resin	83	29.5
Mortar	74.6	6.2

Table 2 Strengthening details of the test beams.

Beam	Number of CFRP rod	Strengthening length (cm)	Filling Material	Strengthening Position	SL/BL[3]
CB	----	----	----	----	----
BC1(270-SR)	2Ø6	270	Resin	S[1]	0.94
BC2(210-SR)	2Ø6	210	Resin	S	0.56
BC3(270-SM)	2Ø6	270	Mortar	S	0.94
BC4(210-SM)	2Ø6	210	Mortar	S	0.56
BC5(270-UR)	2Ø6	270	Resin	U[2] (+20mm)	0.94

(1) S: on the same level of the steel bars.
(2) U: above than steel level.
(3) SL/BL: is the ratio between strengthening length SL and beam length BL, where SL is the distance between the end of the CFRP bar and the applied load and BL is the distance between the support and the applied load

Table 3 Experimental results of the test beams

Beam	Failure Mode	Cracking load, P_{cr}(kN)	Yielding Load, P_y(kN)	Failure Load, P_u(kN)	Strain of CFRP [1] (mm/mm)	χ[2]	Strain of steel [3] (mm/mm)	E_{ab}
CB	Conventional flexural failure	17.1	64.3	72.8	----	-----	0.0193	2702.5
BC1(270-SR)	1	18.3	90	116.0	0.0069	0.54	0.0082	4583.8
BC2(210-SR)	3	17.3	94.5	106.4	0.0042	0.33	0.0043	1586.1
BC3(270-SM)	2	18.0	81.8 (88)*	106.0	0.0064	0.50	0.0035	2951.2
BC4(210-SM)	2	18.8	92.4	94.1	0.0028	0.22	0.0033	972.0
BC5(270-UR)	1	17.8	83.2	102.7	0.0041	0.32	0.0104	3267.9

(1)Strain of CFRP: the recorded strain in CFRP rods at failure load of a strengthened beam.
(2)χ : Efficiency ratio of the CFRP rods = (Strain of CFRP (1) / ε_{fu}) .
ε_{fu}: Ultimate tensile strain of CFRP rod obtained from axial testing of three specimens $= 0.0128\ mm/mm$.
(3)Strain of steel: recorded strain in steel bars at failure load of a strengthened beam.
(4)E_{ab}: Energy absorption capacity.
**Adjusted value, determined by considering 5% variation from BC4*

Table 4 Mid-span deflection and ductility of the tested beams

Beam	δ_y **(1)** **(mm)**	δ_u **(2)** **(mm)**	μ **(3)**
CB	13.4	59.3	4.43
BC1(270-SR)	15.5	50.4	3.25
BC2(210-SR)	15.5	22.9	1.48
BC3(270-SM)	15.7 (16.5)*	38.2	2.43 (2.31)*
BC4(210-SM)	15.8	16.2	1.03
BC5(270-UR)	13.6	40.4	2.97

(1) δ_y: Mid-span deflection of beam at level of yielding load attained from Fig.4.
(2) δ_u: Mid-span deflection of beam at level of failure load attained from Fig.4.
(3) μ (ductility index) = Ultimate deflection (δ_u) / Yielding deflection (δ_y).
**According to the adjusted value (Table 3)*

Table 5 Comparison between experimental results of the SNSM and NSM techniques

SNSM technique						NSM technique [6]					
Beam	**Failure mode**	**M_{cr} (1) (kN.m)**	**M_y (2) (kN.m)**	**M_u (3) (kN.m)**	**μ (4)**	**Beam**	**Failure mode**	**M_{cr} (kN.m)**	**M_y (kN.m)**	**M_u (kN.m)**	**μ**
BC1(270-SR)	Crushing of the compressed concrete nearby the load application.	7.3	36	46.4	3.3	S-C 6 (270-R)	CFRP rod pull-out	7.4	36.8	53.3	2.9
BC2(210-SR)	Concrete peeling-off at the end of CFRP rod.	6.9	37.8	42.6	1.5	S-C 6 (210-R)	Concrete peeling-off at the end of CFRP rods	8.1	38.2	44.0	1.5
BC3(270-SM)	Debonding at the mortar–concrete interface together with compressed concrete crushing.	7.2	32.7 (35.2)*	42.4	2.4 (2.3)*	S-C 6 (270-M)	Debonding at the mortar–concrete interface	8.1	35.3	43.9	1.9
BC4(210-SM)	Debonding at the mortar–concrete interface followed by compressed concrete crushing.	7.5	36.9	37.7	1	------	------	-----	-----	-----	-----
BC5(270-UR)	Crushing of the compressed concrete near to the load application.	7.1	33.3	41.1	3	S-C 6 (270-R)	CFRP rod pull-out	7.4	36.8	53.3	2.9

(1) M_{cr} (cracking moment) = $\frac{P_{cr}}{2} * a$, where P_{cr} is the cracking load of the beam obtained from experimental test (Table 3) and a = 800mm.

(2) M_y (yielding moment) = $\frac{P_y}{2} * a$; where P_y is the yielding load of the beam obtained from experimental test (Table 3) and a = 800mm.

(3) M_u (ultimate moment) = $\frac{P_u}{2} * a$; where P_u is the ultimate load of the beam obtained from experimental test (Table 3) and a = 800mm.

(4) μ (ductility index): (Table 4)

**According to the adjusted value (Table 3)*